FINAL REPORT

NASA Planetary Atmospheres Proposal (NAG5-6796)
"The Coupled Roles of Dust and Clouds in the Mars Climate"

P.I.-R. Todd Clancy
Space Science Institute, P.O. Box 3075, Bald Head Island, NC 28461
(910) 457-6362, clancyr@colorado.edu

I proposed that the "wind down" funding from Planetary Atmospheres be targeted towards concluding the microwave studies of the Mars atmosphere I have conducted since 1988. This wind down effort centered on publication of existing Mars millimeter observations and their comparison to ongoing MGS Thermal Emission Spectrometer (TES) temperature measurements. It also provided for the analysis of scheduled Kitt Peak and JCMT Mars observations through March 1999, for a more complete seasonal comparison to TES and to complete five full Mars years of contiguous observations.

1) Completed MGS/TES Comparisons- It has been suggested that the microwave temperature profiling of Mars has underestimated Mars atmospheric temperatures by 15-20K, based on comparisons to Viking descent profiles, Viking IRTM observations, and most recently from Pathfinder descent profile observations (Schofield et al., 1997). In fact, a reanalysis of the Viking IRTM 15 micron data (Wilson and Richardson, 1999) places these global 0.5 mbar (~25km) atmospheric temperatures virtually on top of the microwave temperatures, particularly for the critical aphelion season (Ls around 70). So now a significant Viking data set has become supportive of the redefinition of the current Mars climate as the cold and cloudy (i.e., less dusty) state determined from the long-term microwave temperature and water vapor measurements (Clancy et al., 1996).

Clearly, contemporaneous comparisons between microwave observations and the MGS TES IR observations are extremely valuable for settling this controversy and so determining the basic character and processes which control the current Mars climate. There exists a special opportunity for such comparisons because frequent (every 3 days) microwave and TES (every orbit) observations were taken from Sep97 to Mar98, in support of MGS aerobraking. Furthermore, extended comparisons between MGS mapping observations over 98-99 with new Kitt Peak and JCMT observations through June 1999 has provided nearly complete seasonal coverage for the TES-microwave comparisons, including the critical aphelion season in 1999 (when the MGS mapping mission began).

The complete set of microwave temperatures are now published. Key issues addressed in these data include the recurrence of global atmospheric warmings associated with perihelion dust storms in four consecutive Mars years, the repeatability of the cold aphelion climate in all Mars years, water profile observations (from the VLA and Kitt Peak) in 1997-99, and the MGS/microwave comparisons in 1997-99.

2) Attached Publications- Published manuscripts associated with the proposed millimeter/TES comparisons (Clancy et al., 2000) and their implications for the Mars climate (Clancy, 1999) are attached below. These publications serve as the fundamental products of this completed Planetary Atmospheres research project.

3) References- Clancy et al., Water vapor saturation at low altitudes around Mars aphelion: A key to Mars climate?, *Icarus*, **122**, 36-62, 1996; Clancy, R.T., Orbital and Interannual Variability of the Global Mars Climate, *5th International Mars Conference*, Pasadena, CA, July 1999; Clancy, R.T., B.J. Sandor, P.R. Christensen, M.D. Smith, J.C. Pearl, B.J. Conrath, and M.J.Wolff, An inter-comparison of ground-based millimeter, MGS TES, and Viking atmospheric temperature measurements: Seasonal and interannual variability of temperatures and dust loading in the global Mars atmosphere, *J. Geophys. Res.*, **105**, 9553-9572, 2000.; Schofield et al., The Mars Pathfinder Atmospheric Structure Investigation/Meteorology Experiment (ASI/MET), *Science*, **278**, 1758, 1997; Wilson and Richardson, Comparison of GCM results with the Viking and Mariner 9 data and implications for the interpretation of MGS atmospheric temperature data , *J. Geophys. Res.*, in press, 2000.

An intercomparison of ground-based millimeter, MGS TES, and Viking atmospheric temperature measurements: Seasonal and interannual variability of temperatures and dust loading in the global Mars atmosphere

R. T. Clancy,[1] B. J. Sandor,[2] M. J. Wolff,[1] P. R. Christensen,[3] M. D. Smith,[4] J. C. Pearl,[4] B. J. Conrath,[5] and R. J. Wilson[6]

[1]Space Science Institute, Boulder, Colorado.

[2]National Center for Atmospheric Research, Boulder, Colorado.

[3]Geology Department, Arizona State University, Tempe.

[4]Goddard Space Flight Center, Greenbelt, Maryland.

[5]Astronomy Department, Cornell University, Ithaca, New York.

[6]Geophysical Fluid Dynamics Laboratory (NOAA), Princeton, New Jersey.

Appeared in Journal of Geophysical Research (Planets), 104, (E4), 9,553-9,572.

Abstract. During the period October 1997 to September 1999 we obtained and analyzed over 100 millimeter-wave observations of Mars atmospheric CO line absorption for atmospheric temperature profiles. These measurements extend through one full Mars year (solar longitudes L_S of 190° in 1997 to 180° in 1999) and coincide with atmospheric temperature profile and dust column measurements from the Thermal Emission Spectrometer (TES) experiment on board the Mars Global Surveyor (MGS) spacecraft. A comparison of Mars atmospheric temperatures retrieved by these distinct methods provides the first opportunity to place the long-term (1982-1999) millimeter retrievals of Mars atmospheric temperatures within the context of contemporaneous, spatially mapped spacecraft observations. Profile comparisons of 0-30 km altitude atmospheric temperatures retrieved with the two techniques agree typically to within the 5 K calibration accuracy of the millimeter observations. At the 0.5 mbar pressure level (~25 km altitude) the 30°N/30°S average for TES infrared temperatures and the disk-averaged millimeter temperatures are also well correlated in their seasonal and dust-storm-related variations over the 1997-1999 period. This period includes the Noachis Terra regional dust storm, which led to very abrupt heating (~15 K at 0.5 mbar) of the global Mars atmosphere at L_S=224° in 1997 [*Christensen et al.*, 1998; *Conrath et al.*, this issue; *Smith et al.*, this issue]. Much colder (10-20 K) global atmospheric temperatures were observed during the 1997 versus 1977 perihelion periods (L_S=200°-330°), consistent with the much (2 to 8 times) lower global dust loading of the atmosphere during the 1997 perihelion dust storm season versus the Viking period of the 1977a,b storms. The 1998-1999 Mars atmosphere revealed by both the millimeter and TES observations is also 10-15 K colder than presented by the Viking climatology during the aphelion season (L_S=0°-180°, northern spring/summer) of Mars. We reassess the observational basis of the Viking dusty-warm climatology for this season to conclude that the global aphelion atmosphere of Mars is colder, less dusty, and cloudier than indicated by the established Viking climatology even for the Viking period. We also conclude that Mars atmospheric temperatures exhibit their most significant interannual variations during the perihelion dust storm season (10-20 K for L_S=200°-340°) and during the post-aphelion northern summer season (5-10 K for L_S=100°-200°).

1. Introduction

The successful orbit insertion of Mars Global Surveyor (MGS) in early September of 1997 marked the beginning of the most significant spacecraft exploration of Mars since the Viking orbiter observations in the late 1970s. One of the unique aspects of the MGS mission is its use of aerobraking to obtain the circular, fixed local-time orbit for mapping operations. In support of this MGS aerobraking, a coordinated program of Mars atmospheric monitoring was developed to provide quantitative, real-time assessment of atmospheric density variations at the altitudes of aerobraking. This program included a broad range of spacecraft and ground-based observations as well as several modeling efforts [*Keating et al.*, 1998]. The following analysis presents an intercomparison between two of the aerobraking observational data sets, both pertaining to Mars atmospheric temperatures over the 0-30 km altitude range for the period October 1997 through September 1999. The specific concern of this comparison is the degree to which the global average behaviors of temperatures and dust loading in the lower Mars atmosphere are described by a relatively dusty, warm model based largely on Viking lander measurements [e.g., *Haberle et al.*, 1993, 1997; *Schofield et al.*, 1997] or the colder, less dusty behavior determined from 1980s and 1990s ground-based observations [*Clancy et al.*, 1990, 1996]. The broader implications of these divergent climate descriptions include fundamental issues of dust-ice aerosol interactions, interannual and seasonal variability, photochemistry, and meridional transport of water and dust in the current Mars climate system [*Clancy et al.*, 1996; *Clancy and Nair*, 1996].

The relevant MGS data set is provided by the Thermal Emission Spectrometer (TES) [*Christensen et al.*, 1992], which measures spectrally resolved brightness temperatures across the 15 μm CO_2 absorption/emission band. Radiances in the CO_2 band are inverted to profile Mars atmospheric temperatures in both nadir and limb pointing geometries [*Christensen et al.*, 1992, 1998; *Conrath et al.*, this issue]. While the TES limb observations allow temperature retrievals to higher altitudes (~60 km), they provide much reduced temporal and spatial coverage (during the aerobraking period) as compared to the TES nadir observations. Consequently, the current comparison employs only the TES nadir temperature profiling over the 0-30 km altitude range. *Christensen et al.* [1998], *Smith et al.* [this issue], *Conrath et al.* [this issue] and J. C.Pearl et al. (Mars water ice clouds: Observations by the Thermal Emission Spectrometer (TES) during the first Martian year, submitted to *Journal of Geophysical Research*, 1999) present the broader range of the TES atmospheric results from the initial aerobraking operations, including nadir and limb measurements of atmospheric temperatures and aerosols.

The second comparison data set is provided by ground-based millimeter CO line retrievals of disk-averaged Mars atmospheric temperature profiles over the 0-80 km altitude region, as observed from Kitt Peak, Arizona (National Radio Astronomy Observatory (NRAO) 12 m telescope for millimeter spectroscopic studies, operated by Associated Universities, Inc., under cooperative agreement with the National Science Foundation). This technique employs the optically thick line opacities from rotational transitions of CO in its ground vibrational state at millimeter to submillimeter wavelengths, to sound atmospheric temperatures in essentially the same manner as infrared CO_2 remote soundings are employed. Significant differences, relative to the infrared radiation, include the linear temperature dependence of emission, the separation of individual rotational lines, and the negligible role of aerosol scattering/absorption at millimeter wavelengths. Because of the small angular size of Mars (4″-20″) and the diffraction limited resolution of millimeter telescopic observations (~15″-60″), millimeter temperature retrievals typically yield low- to midlatitude, dayside averages for the Mars atmosphere. The altitude range sounded extends from the surface to as high as 80 km, depending on the rotational transition observed and the signal-to-noise ratios obtained. A more detailed description of the method and prior results have been published elsewhere [*Clancy et al.*, 1983, 1990, 1996; *Clancy and Sandor*, 1998].

2. Comparison Goals

The distinct differences in the TES and millimeter spatial resolutions and latitude/longitude sampling versus time (diurnal, daily, and seasonal) are significant obstacles to a detailed statistical comparison of these temperature retrievals. Fortunately, such precise comparisons are not required to obtain important results. This is because the Mars atmospheric issues raised by these millimeter retrievals correspond to large temperature differences with respect to the Viking climatology (15-20 K) and so can be addressed with millimeter-TES comparisons of relatively modest accuracy (e.g., 3-5 K). Our first comparison goal is to determine the average thermal state of the global Mars atmosphere as described by the millimeter and TES temperature retrievals. The specific measurement issue is the 15-20 K offset between the 1982-1999 ground-based millimeter and the 1976 Viking and 1997 Pathfinder descent profile retrievals of Mars atmospheric temperatures over the 0-50 km altitude range. The warmer Viking and Pathfinder entry profiles are very limited in temporal and spatial coverage (three profile measurements at 19°, 22°, and 44° N, for L_S=96°, 117°, and 143° respectively), but have been interpreted as typical of minimum atmospheric dust loading and hence minimum atmospheric temperatures. The Viking model of Mars climate is based on these entry profiles and seasonally extended Viking observations (e.g., the 15 μm IRTM maps [*Martin*, 1981] and the lander dust opacity determinations [*Colburn et al.*, 1989]) of a relatively warm Mars atmosphere, in which vertically extended dust loading equivalent to column visible opacities of $\geq$0.5 characterizes Mars low- to midlatitudes in all seasons [e.g., *Pollack et al.*, 1979; *Haberle et al.*, 1997]. The Pathfinder imaging [*Smith et al.*, 1997; *Smith and Lemmon*, 1999] and descent entry teams [*Schofield et al.*, 1997] conclude that the millimeter temperatures are biased 15-20 K cold and that dusty, warm conditions are a constant condition of the current Mars climate, although the presence of a deep temperature inversion in the lower scale height suggests some distinction from the Viking description [*Magalhães et al.*, 1999; *Colaprete et al.*, 1999; see also *Titov et al.*, 1999].

However, the Viking model of the Mars atmosphere may be inaccurate even for the Viking period. *Wilson and Richardson* [2000] present evidence for a positive bias in the Viking IRTM 15 μm radiances due to an unaccounted contribution from surface emission. We refer readers to *Wilson and Richardson* [2000] for a complete description of the differences and origins of the corrected versus uncorrected IRTM temperatures, but the correction stems from an apparent out-of-band leak in the Viking IRTM 15 μm channel filter response, which leads to substantial contribution from diurnal and latitude-dependent Mars surface emission. An important consequence of this correction is that Mars atmospheric temperatures during the Viking period become more comparable to the millimeter record of Mars atmospheric temperatures over the past 10 years [see also *Richardson*, 1998]. The presented millimeter-TES comparison provides the first opportunity to verify the 5 K absolute accuracy of the millimeter retrievals [*Clancy et al.*, 1996], and so establish a baseline for the thermal and aerosol conditions of the Mars atmosphere versus solar longitude (L_S) over the 1990s. In our comparison of these conditions to the Viking and Mariner 9 periods, we consider how the corrected Viking IRTM 15 μm temperatures and a review of IRTM 9 μm dust opacities [*Martin*, 1986] may support a colder and less dusty (in terms of background dust loading) model of the Viking period atmosphere which compares more closely with currently observed conditions. This also allows a more accurate definition of interannual variations implied by the remaining differences between the Viking and current periods.

The second comparison goal is an assessment of the spatial scale of temporal variations that have been observed in the long-term millimeter measurements. This includes a very repeatable 20-30 K orbital variation in Mars disk-averaged atmospheric temperatures, which is roughly twice that exhibited by the warm, dusty Viking-based model of the low- to midlatitude Mars atmosphere. Additionally, very rapid (approximately a few days) temperature increases of 10-20 K have been observed in all Mars southern summer seasons observed [e.g., *Clancy et al.*, 1994], and within many northern summer seasons

as well [*Clancy*, 1996]. Both kinds of atmospheric temperature increases exhibit specific temporal and altitude dependencies, which have been attributed to global-scale dust heating and dust-ice aerosol interactions within the Mars atmosphere. A key uncertainty in this interpretation is the degree to which such variations in disk-averaged measurements represent globally coherent variations of atmospheric temperatures on Mars. For example, do perihelion 15 K increases in disk-averaged temperatures at 10-50 km altitudes correspond to latitude-independent 15 K temperature increases over low- to midlatitudes? Or do they represent a weighted average of much larger temperature increases in the northern hemisphere middle atmosphere which are compensated in the disk average by temperature decreases in the southern hemisphere middle atmosphere? The TES mapping observations are ideally suited to placing the long-term millimeter record of Mars atmospheric temperature variations in a physically interpretable context.

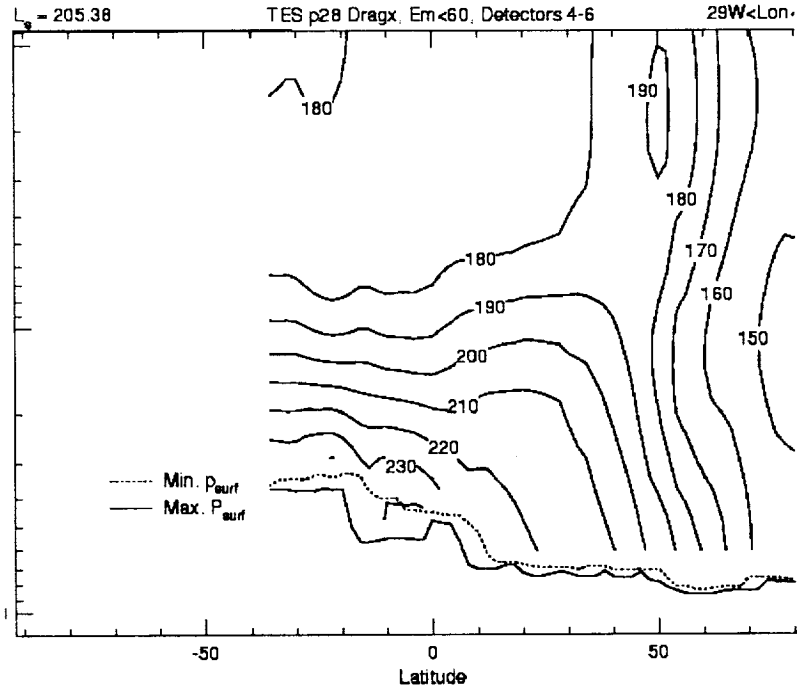

Figure 1. Latitude-pressure contour of Mars atmospheric temperatures as retrieved from TES observations in October 1997 (L_S=205°, orbit 28, longitudes 29°-50° W). The altitude range corresponding to the 7-0.1 mbar pressure range is roughly 0-30 km. Such TES latitudinal cross sections are averaged according to the latitudinal weighting of the millimeter whole-disk measurements to provide the TES-millimeter profile comparisons of Figures 2-5 and 7-8.

3. Temperature Comparisons

3.1. Perihelion Temperature Profiles (0-30 km altitudes)

Millimeter-TES comparisons of temperature profiles (0-30 km altitudes) are presented for six observational periods extending from L_S=205°-214° in 1997 to L_S= 141°-144° in 1999. Three perihelion periods are selected to present southern spring/summer conditions before (L_S=205°-214°), during (L_S=226°-227°), and after (L_S=300°-308°) the 1997 Noachis Terra regional dust storm (beginning at L_S=224°) [*Smith et al.*, 1999). We also present three aphelion comparisons for the northern

spring/summer season (L_S=28°-34°, 108°-112°, and 141°-144°), which allow seasonally equivalent comparisons to the Viking [*Seiff and Kirk*, 1977] and the Pathfinder [*Magalhães et al.*, 1999] descent profile measurements. As the L_S=40°-100° seasonal range was not observed by TES, we include a millimeter profile comparison to MGS (D. P. Hinson, private communication; see also *Hinson et al.* [1999]) and Viking [*Lindal et al.*, 1979] radio occultation profiles obtained over L_S=74°-77°. Uncorrected Viking IRTM 15 μm measurements of global (dayside) atmospheric temperatures near the 0.5 mbar pressure level (~25 km altitude) are indicated to demonstrate the seasonal behavior of the Viking-based climatology. Corrected IRTM values of atmospheric temperature are included to indicate the significance of the revision proposed by *Wilson and Richardson* [2000] for this key Viking atmospheric measurement.

Table 1. Observational Parameters for TES Infrared and Kitt Peak Millimeter Comparisons of Mars Temperature Profiles (for Figures 2-8)

L_S,°	Date	TES Orbit	KP LAT$_{SE}$	TES LAT	KP LONG$_{SE}$	TES LONG	KP LT$_{SE}$	TES LT
206	10/27/97	28	···	40° S-80° N	···	30°-50°	···	19.1
209	10/31/97	···	1° N	···	295°-330°	···	10.2	···
213	11/07/97	36	···	50° S-85° N	···	195°-245°	···	16.5
214	11/09/97	···	2° S	···	175°-230°	···	10.2	···
227	11/30/97	52	···	60° S-85° N	···	110°-200°	···	15.6
227	11/30/97	···	9° S	···	340°-30°	···	10.3	···
228	12/01/97	53	···	55° S-85° N	···	200°-315°	···	15.6
300	03/27/98	···	24° S	···	220°-270°	···	11.5	···
304	04/04/98	215	···	45° S-85° N	···	240°-255°	···	10.3
308	04/08/98	···	22° S	···	100°-170°	···	11.6	···
29	09/10/98	550	···	5° N-85° N	···	190° – 200° 10° – 20°	···	17.5,5.5
34	09/24/98	···	22° N	···	220°-250°	···	13.5	···
108	03/10/99	1691-1702	···	60° S-70° N	···	0°-360°	···	2,14
111	03/16/99	···	15° N	···	250°-280°	···	13.8	···
141	05/19/99	2543-2554	···	70° S-85° N	···	0°-360°	···	2,14
144	05/25/99	···	23° N	···	270°-320°	···	10.4	···

KP, Kitt Peak. Read 10/27/97 as October 27, 1997. Longitude convention is West.

Each of the TES-millimeter profile comparisons incorporate our best efforts to construct latitudinal averages of the spatially resolved TES temperatures, which correspond most directly to the latitudinal weighting of the disk-averaged, ground-based measurements. The longitudinal and local time coverage of the TES and millimeter observations are distinct in sampling, and often separated in specific coverage. The millimeter whole-disk measurements average over a wide range of longitudes and dayside local times in each observation, where the sub-earth longitude cycles within a 1 month period. During the aerobraking phase, the TES latitudinal maps tend to cover relatively narrow (10°) longitude and local time ranges, and the subspacecraft longitudes vary rapidly per orbit and versus time. For example, the longitudinal coverage for the TES temperatures obtained on the early orbit 28 (Figure 1; October 27, L_S=205.8°) is 30°-50° W, and the latitudinal coverage extends from 40° S to high northern latitudes.

However, TES observations during the mapping phase (past L_S=100°) incorporate full longitudinal coverage and two local times (0200 and 1400 LT). Comparisons of the Mars season (L_S), longitudes, local times, and sub-Earth latitudes for both sets of observations are presented in Table 1.

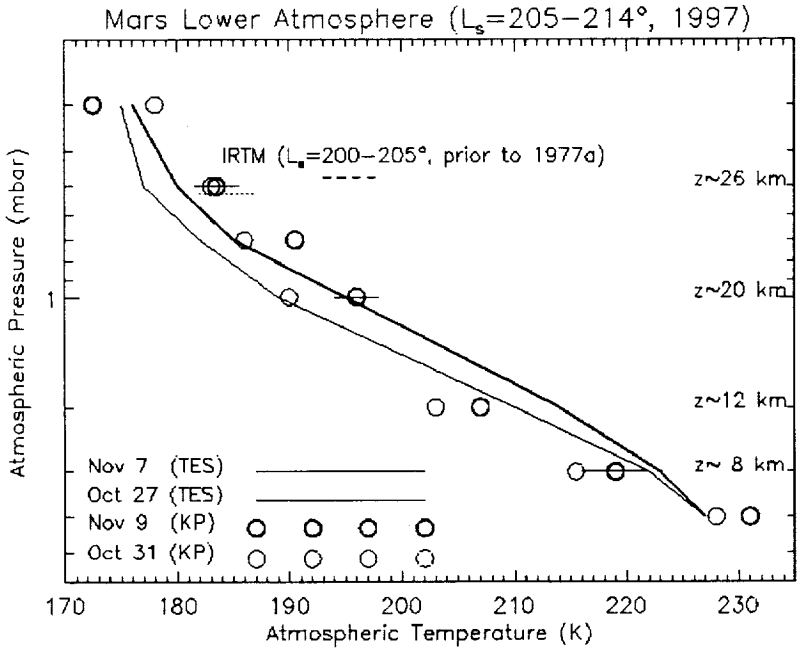

Figure 2. TES (lines) and millimeter (circles) temperature profiles obtained in October-November of 1997 (L_S=205°-214°), prior to the Noachis Terra regional dust storm. The TES profiles are latitudinal averages, obtained from extended TES latitudinal coverage (such as Figure 1) and weighted corresponding to the whole-disk averaging of the ground-based millimeter observations (primarily low- to midlatitudes). For comparison, the 0.5 mbar temperatures from the Viking IRTM experiment over L_S range 200°-205° (pre-1977a storm) in 1976-1978 are indicated by dashed (original) and dotted (modified according to ***Wilson and Richardson*** [2000]) lines. The dates, longitudes, local times, and sub-earth latitudes for these averages are indicated in Table 1. Several altitude levels corresponding to the atmospheric pressure coordinate are indicated on the right.

Figure 2 presents the L_S=205°-214° comparison of TES and millimeter temperature profiles, corresponding to the early period of MGS aerobraking. The TES profiles are latitudinal averages calculated to approximate the whole-disk averaging present in the millimeter observations. The natural vertical coordinate for the TES and millimeter retrievals is atmospheric pressure, but we indicate approximate altitude levels on the right-hand vertical side of the figure. The TES temperatures for orbits 28 (thin line) and 36 (thick line), correspond to L_S of 205.8° and 213.0°, respectively. These compare to L_S of 208.8° and 214.2° for the October 31 (thin circles) and November 9 (thick circles) millimeter profiles. Hence the closest comparisons between two data sets in terms of time are orbit 28 versus October 31 (separated by 4 days), and orbit 36 versus November 9 (separated by 1.5 days). For comparison, we have included the range of IRTM 15 μm temperatures (30° S-30° N, 0700-1800 LT, referenced to the 0.5 mbar atmospheric pressure [*Kieffer et al.*, 1976]) for L_S=200°-205° in 1977, prior to the heavy dust loading marked by the 1977a storm. The dashed range presents the original IRTM temperatures, and the dotted line region indicates the cooler IRTM temperatures resulting from the

Wilson and Richardson [2000] correction for a modeled contamination from surface emission.

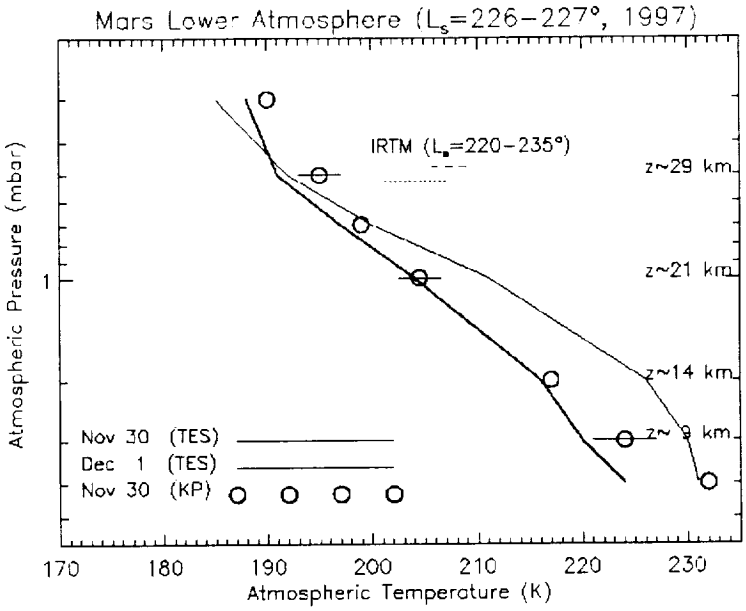

Figure 3. TES (lines) and millimeter (circles) temperature profiles obtained in November-December of 1997 (L_S=226°-227°), during the Noachis Terra regional dust storm. Figure description same as for Figure 2.

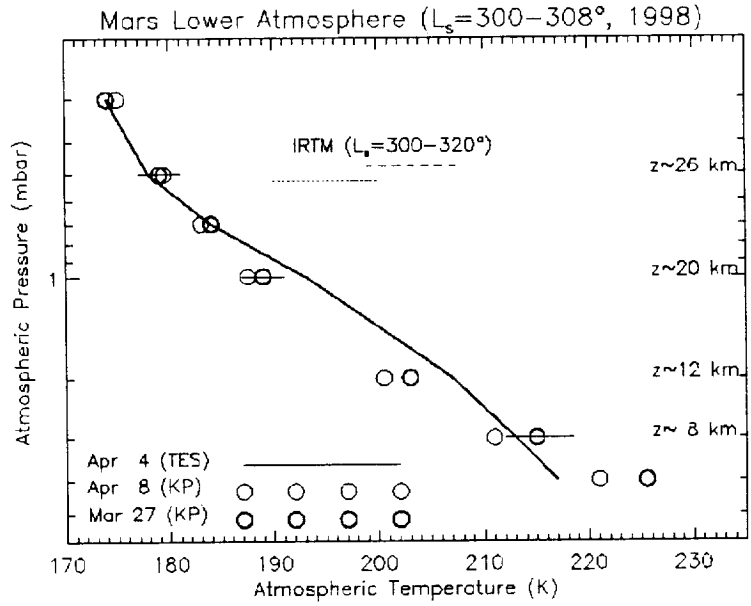

Figure 4. TES (lines) and millimeter (circles) temperature profiles obtained in March-April of 1998 (L_S=300°-308°), toward the end of the first phase of MGS aerobraking. Figure description same as for Figure 2.

Figure 3 presents two TES profiles and one millimeter profile taken just after the onset of the Noachis Terra regional dust storm in November of 1997 (L_S=226°-227°). These profiles indicate maximum global atmospheric temperatures observed in the TES and millimeter measurements over the 1997-1998 period. The distinctions in lower atmospheric temperatures for TES orbits 52 and 53 are probably related to longitudinal variations, but there is a 1 day offset in time between these orbits. The IRTM temperatures at L_S=220°-234° in 1977 remain 10-15 K warmer than at the peak of the 1997 Noachis Terra regional dust storm. Figure 4 presents two Kitt Peak and one TES profile for the L_S=300°308° period in the spring of 1998, which is near the end of the first phase of MGS aerobraking (latitudinal coverage degraded considerably in the second aerobraking period of August-October 1998). The TES and millimeter profiles for this L_S=300°-308° period present similar temperatures to the L_S=205°-214° season 5 months earlier, although the lowermost 10 km is slightly cooler. The IRTM correction (dotted versus dashed lines) is significant (~10 K), but the L_S=300°-308° period in 1977 is significantly warmer (10-25 K) than the L_S=300°-308° period in 1998 for either case, as a consequence of the late and very intense 1977b storm.

3.2. Aphelion Temperature Profiles (0-30 km altitudes)

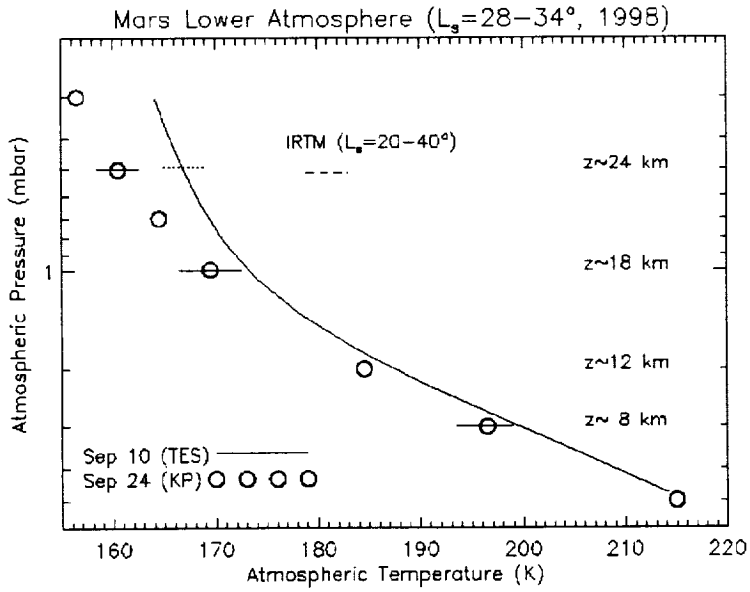

Figure 5. TES (lines) and millimeter (circles) temperature profiles obtained in September of 1998 (L_S=28°-34°) during the early northern spring when global atmospheric temperatures are falling and TES coverage is more limited. Figure description same as for Figure 2.

Figure 5 compares an L_S=34° Kitt Peak profile to TES temperature measurements obtained on orbit 550 (L_S=28.5°), after completion of MGS aerobraking and before mapping operations commenced. The latitudinal coverage of these northern early spring TES observations are more limited (Table 1) than during aerobraking or mapping observations. In addition, the disk averaging of the Kitt Peak millimeter technique leads to maximum differences from low latitude Mars atmospheric temperatures in early northern spring. The sub-earth latitude lies well northward of the subsolar latitude at this time, such that the disk average incorporates a significant northern latitudinal gradient (10-15 K) in Mars atmospheric temperatures. Millimeter disk-averaged temperatures are 3-4 K colder than Mars low-latitude temperatures at this time, whereas for the other profile comparisons, disk averaged

millimeter temperatures are generally within 1-2 K of Mars low-latitude temperatures. Disk-averaging of the available TES temperatures at L_S=34° leads to 3-5 K agreement with the presented L_S=34° millimeter profile. The Viking model for this period remains 10-15 K warmer (dashed horizontal line, IRTM), while the *Wilson and Richardson* [2000] correction to these IRTM temperatures (dotted horizontal line) brings all three temperature data sets within 5 K of one another.

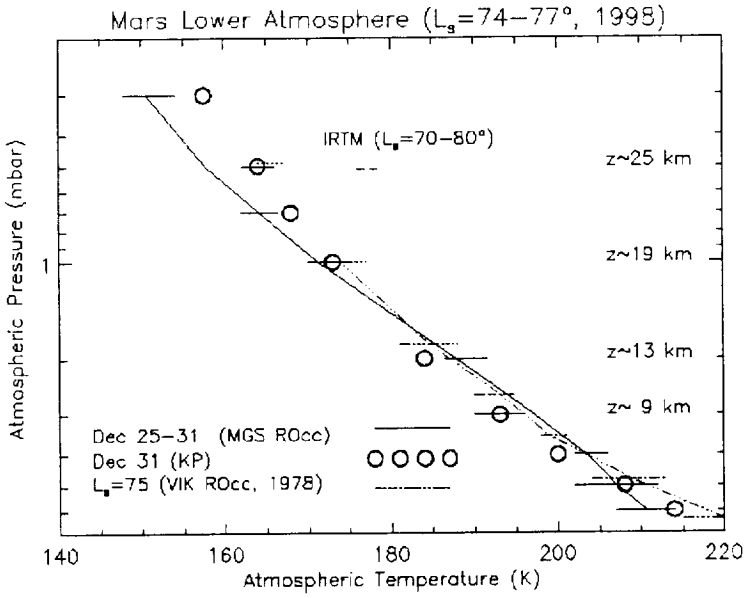

Figure 6. A millimeter (circles) temperature profile from December of 1998 (L_S=77°, LAT_{se}=22° N, LT_{se}=1430) is compared to the average of three low-latitude Viking radio occultation profiles (dash-dotted line: L_S=74°, LAT=27° N, LT=1600, 1978), and to the average of 10 high-latitude MGS radio occultation profiles (solid line: L_S=76°, LAT=67° N, LT=0400, 1998).

MGS operations were greatly reduced between the end of aerobraking and the beginning of the mapping mission (March 1999), such that TES observations were not obtained over the L_S=40°-100° period of Mars aphelion passage (at L_S=71°). However, MGS radio occultation profiles were returned over L_S=74°-77° at Mars high northern latitudes (64°-67° N) at the end of 1998 (unpublished data provided by D. P. Hinson and the MGS Radio Science Team). There also exists for this season in 1978 a set of three Viking radio occultation profiles measured in the vicinity of the Viking 1 lander site [*Lindal et al.*, 1979]. As shown in Figure 6, average temperature profiles from these MGS (solid line) and Viking (dash-dotted line) radio occultations are remarkably similar, despite their differences in latitude (65° N versus 27° N) and local time (0400 versus 1600 LT). In fact, global circulation model (GCM) atmospheric temperature fields predict very weak (1-3 K) latitudinal gradients between the equator and 70° N at aphelion, and TES temperature fields obtained at L_S=108° (see below) show similarly weak latitudinal gradients over the northern early summer hemisphere. GCM tides also show weak diurnal variations between these two measurements. In this spirit we present an L_S=77° millimeter profile obtained on December 31, 1998 (LAT_{se}=22° N, LT_{se}=1430) for comparison to the 1998 MGS and 1978 Viking radio occultation profiles for this season. While this comparison is not as direct as the coincident, contemporaneous TES-millimeter comparisons, the 1-5 K agreement among the aphelion temperature profiles of Figure 6 is significant. The MGS radio occultation measurements are contemporaneous with the millimeter profile measurement. The Viking radio occultation profiles

demonstrate that aphelion atmospheric temperatures during the Viking period were as cold as the millimeter aphelion measurements over the Viking 1 lander site, at least for the duration of these Viking radio occultation observations (2 days).

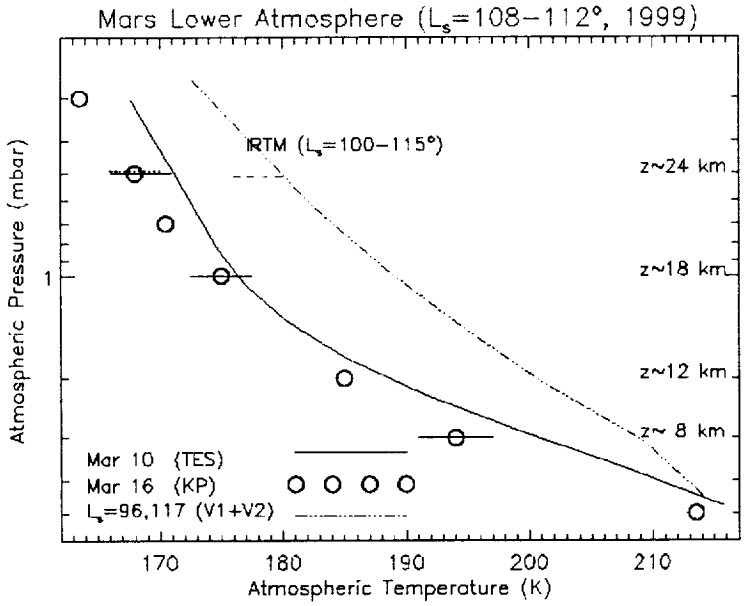

Figure 7. TES (lines) and millimeter (circles) temperature profiles obtained in March of 1999 (L_S=108°-112°), at the beginning of the MGS mapping mission. The dash-dotted profile presents the averaged Viking 1 (22° N, 1600 LT) and 2 (48° N, 0400 LT) lander descent measurements. Figure description same as for Figure 2.

TES mapping operations, which began in early March of 1999, provide complete zonal averaging and local time coverage of 0200 and 1400 LT. The availability of these mapping data is recent relative to the publication of this paper, but several periods have been provided for comparison to the millimeter 1999 observations. Figure 7 presents a millimeter-TES profile comparison for the L_S=108°-112° period in mid-March of 1999. This seasonal range is suitable for comparison to the average temperature profile (dash-dotted line) from the Viking 1 (22° N, 1600 LT, L_S=96°) and 2 (48° N, 0900 LT, L_S=117°) lander descent observations. For altitudes above 5 km, TES-millimeter temperatures agree to within 2-6 K, whereas the average of the Viking lander profiles lies 10-13 K above the TES profile. The corrected IRTM temperatures (dotted horizontal line at 0.5 mbar) also show closer agreement with the TES and millimeter observations, relative to the uncorrected IRTM temperatures (dashed horizontal line).

Figure 8 presents a late northern summer comparison (L_S=141°-144°) of TES, millimeter, and Pathfinder temperature profiles. The millimeter temperatures are biased ~4 K colder than the TES temperatures over the 0-30 km altitude region, which is similar to comparison results for the northern spring and summer periods of Figures 5 and 7. Also similar to the Viking descent profile comparison of figure 7, Pathfinder temperatures are 10-13 K warmer than the TES temperatures, although only for altitudes above ~17 km. Pathfinder temperatures actually fall below the millimeter temperatures at the 8 km lower boundary of the Pathfinder retrieval. *Schofield et al.* [1997] and *Magalhães et al.* [1999] argue that the Pathfinder and Viking descent measurements of Mars atmospheric temperatures are

representative of the unchanging dusty, warm background state of the Mars atmosphere. Consequently, they assert that differences between these 1976 and 1997 northern summer measurements must reflect unrecognized diurnal variations in the lower (<15 km) and upper (>50 km, see also [*Clancy and Sandor*, 1998] atmosphere of Mars, as distinguished by the 0400 LT Viking 1 versus 0400 LT Pathfinder descents.

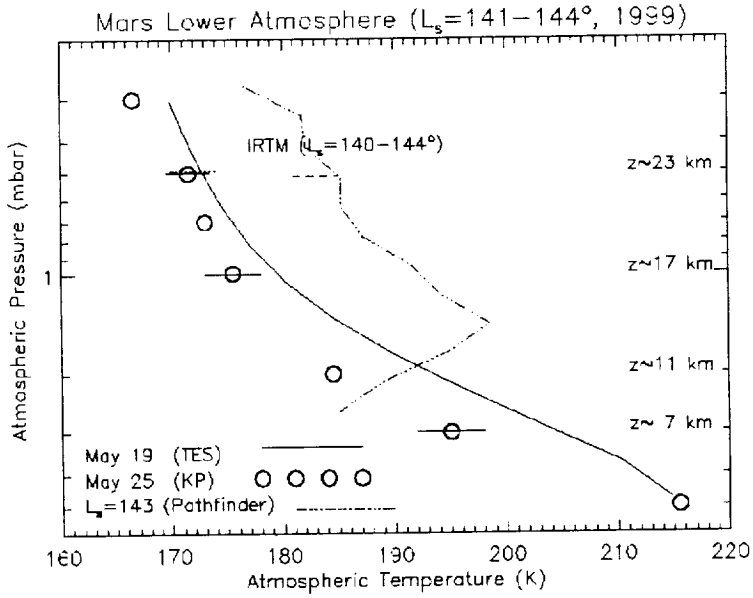

Figure 8. TES (lines) and millimeter (circles) temperature profiles obtained in May of 1999 (L_S=141°-144°), during MGS mapping observations of northern summer. The dash-dotted profile presents the Pathfinder (19° N, 0400 LT) lander descent measurement. Figure description same as for Figure 2.

Colaprete et al. [1999] determined that radiative cooling by a nighttime water ice cloud ($\tau \sim 1$) located near the 10 km altitude level could create the 7-15 km level temperature inversion in the Pathfinder descent profile. However, they note that no evidence of a thick nighttime cloud is present in the Pathfinder aerosol opacity measurements. We point out that the required diurnal forcing for such cloud formation is unsupported and that the 1999 TES profile measurements do not indicate 5-15 km temperature inversions in 0200 LT or 1400 LT measurements. The warm middle atmospheric region observed by Pathfinder may, in fact, reflect locally perturbed conditions associated with a Valles Marineris dust storm observed just days before the Pathfinder landing [*Wolff et al.*, 1999].

Overall, the temperature profile comparisons of Figures 2-8 indicate average differences between the TES and millimeter retrievals that are $\leq$6 K over the 0-30 km altitude region. Specifically, the millimeter-TES differences averaged over the presented three perihelion periods are +4 K for the 5-6 km level, −2 to −5 K for the 9-21 km region, and +1 to +3 K for the 22-30 km region. The millimeter-TES differences averaged over the three presented aphelion periods are −3 to −5 K for the 5-6 km level, −6 to −3 K for the 9-21 km region, and −2 to −4 K for the 22-30 km region. These millimeter-TES differences are substantially smaller than the 15-20 K offset between the millimeter and Viking temperatures. Nevertheless, there does appear to be a 2-5 K cold bias in millimeter relative to TES temperature measurements, particularly for the northern spring/summer period (L_S=20°-160°).

3.3. Dust Storm Effects on TES and Millimeter 0.3 mbar Temperatures

In order to provide more complete coverage of the extended MGS aerobraking period, we present an October 1997 to July 1998 (L_S=190°-360°) time sequence at the 0.3 mbar pressure level (~30 km altitude). For this purpose, we employ comparisons of 30° N and 30° S latitude zonal averages of retrieved TES temperatures to millimeter whole-disk retrievals. TES 0.3 mbar temperatures within ±2.5° latitude of 30° S and 30° N were binned in 30° longitudinal intervals and averaged to provide a consistent temperature trend data set in support of MGS aerobraking operations. Although TES averages at 30° N and 30° S are not precisely equivalent to the spatial averaging of the full-disk millimeter measurements, this 0.3 mbar level comparison provides a reasonably accurate comparison of the TES and millimeter data sets. This is a consequence of modest latitudinal variations in Mars atmospheric temperatures, except over winter high latitudes which are not significantly weighted in the earth-based measurements. The 0.3 mbar level is selected for this comparison because temperatures at this pressure level are a standard product of the TES aerobraking operations, and they exhibit strong sensitivity to dust storm activity. The L_S= 190°-360° range spans the southern hemisphere spring and summer seasons, which exhibit several abrupt increases of dust loading and temperatures in the global Mars atmosphere associated with regional-scale dust storms, including the Noachis Terra regional dust storm [*Smith et al.*, this issue].

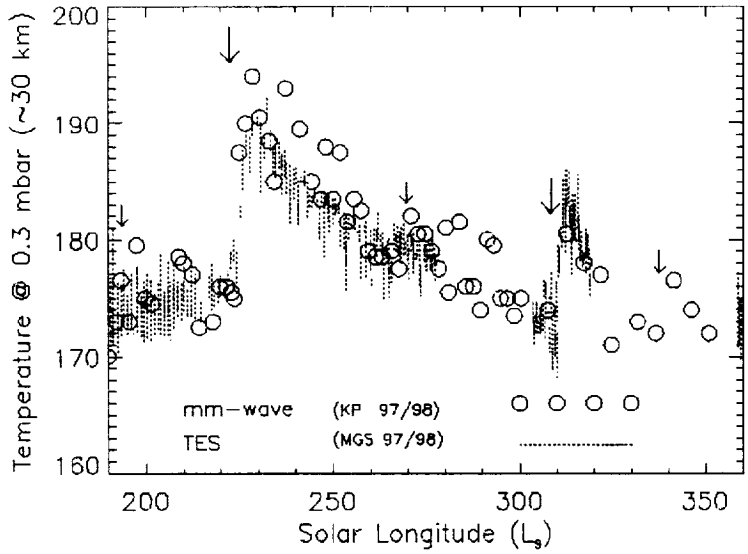

Figure 9. An extended comparison of TES (dotted lines) and millimeter (circles) measurements of Mars atmospheric temperatures for the 0.3 mbar pressure atmospheric pressure level. The full perihelion dust storm season during the 1997-1998 of MGS aerobraking is highlighted (L_S=190° to 360°). The vertical lines plotted for the TES measurements at each point indicate the temperature range between 30°±5° S and 30°±5° N zonal averages. The vertical arrows indicate abrupt increases in atmospheric temperatures and dust loading associated with distinct dust storm activity on Mars, the most intense being the Noachis Terra regional dust storm at L_S=224°[*Smith et al.*, this issue]. Breaks in the TES record correspond to orbital maneuvers and aerobraking periods in which MGS observations were halted.

Figure 9 presents the trend of TES (dashed vertical lines denote the range of 30° S and 30° N values) and millimeter (circles) 0.3 mbar level temperatures for the October 1997 to July 1998 period,

as a function of L_S. The millimeter and TES temperatures differ by typically less than 2-3 K at this ~30 km altitude level over this period of roughly one half of a Mars year. Their temporal variations are also very similar. These close correspondences suggest that the seasonal and short-term variations determined from the long-term (1988-1997) millimeter record are representative of coherent changes in the global atmospheric temperature field rather than of complex changes in the latitudinal distributions of Mars atmospheric temperatures. Vertical arrows mark five distinct atmospheric heating events apparent in the millimeter observations during this period, four of which also appear in the TES temperature and dust opacity measurements (at L_S=190°, 225°, 270°, and 310°). The L_S=225° event is the strongest by far and is associated with the November 1997 Noachis Terra regional storm at southern low- to midlatitudes [*Smith et al.*, this issue]. The weaker temperature increases at L_S=190°, 270°, and 310° have also been identified with regional dust storm activity at southern midlatitudes [*Smith et al.*, this issue]. The L_S=340° temperature increase occurred during a break in TES measurements, associated with the hiatus between the first and second periods of MGS science phasing.

An interesting aspect of these atmospheric heating events is the remarkably short timescale (1-3 days) for global-scale evolution at this 30 km altitude level. The comparable temperature increases in the disk-averaged millimeter and the spatially resolved TES records, and the comparable changes in the 30° S and 30° N TES records both indicate global temperature increases for a vertically extended portion of the Mars atmosphere. Peak temperature increases of the Mars atmosphere during a 1994 global heating event (at L_S=254°) occur at altitude levels of 40-50 km [*Clancy et al.*, 1994]; the current millimeter measurements indicate the same behavior for the 1997-1998 dust storm events. Global temperature increases at altitudes below 0-15 km are significantly smaller, as comparison of Figures 2 and 3 shows. Similarly, although TES dust column opacities increase at northern latitudes during these events, the changes are much smaller than at southern latitudes where the sources are located [*Smith et al.*, this issue]. GCM simulations indicate that strong solar absorption by the deep vertical column of dust at southern latitudes and dynamical heating at northern latitudes associated with the intensification of the Hadley circulation lead to almost latitude-independent temperature increases over the low- to midlatitude range on Mars.

3.4. Seasonal and Interannual Variability of 0.5 mbar Level Atmospheric Temperatures

Plate 1 presents a more comprehensive comparison of Mars atmospheric temperature measurements at the 0.5 mbar pressure level (~25 km altitude), including the previous 2 Mars years (1992-1996) of millimeter observations and the 1970s period of Mariner 9 and Viking observations. This presentation of 0.5 mbar Mars atmospheric temperatures compares 1997-1999 TES (colored dotted lines), 1992-1999 millimeter (colored circles), 1976-1979 Viking IRTM (dotted and dashed lines for corrected and uncorrected values, respectively, and thick and thin lines for 1976-1977 versus 1978-1979), 1976 Viking 1 and 2 descents ($l1$ and $l2$ symbols), Mariner 9 IRIS (cross symbols), and 1997 Pathfinder descent (P symbol) measurements. The 1992-1999 temperature measurements are presented in color (circles for millimeter, dotted lines for TES) to distinguish interannual behavior in the 1992-1999 millimeter temperature record. For the purpose of this comparison, we use the solar longitude range 0°-360° to define a Mars year and adopt April 11, 1955 (L_S=0°) as the beginning of year 1. In this arbitrary convention, the Mariner 9, Viking, Phobos, and Pathfinder missions occurred in years 9-10, 12-15, 19-20, and 23, respectively. By comparison, the 1992-1999 millimeter observations extend over years 21-24, and the 1997-1999 TES observations extend over years 23 and 24.

To first order, the 1992-1999 millimeter temperature record indicates a high degree of repeatability over the past 3.5 Mars years. Earlier millimeter observations show that this repeatability has extended over the past 5-6 Mars years (since 1988 [*Clancy et al.*, 1996]). The uncorrected IRTM temperatures (solid lines), which are indicative of the long-standing Viking model of Mars atmospheric behavior,

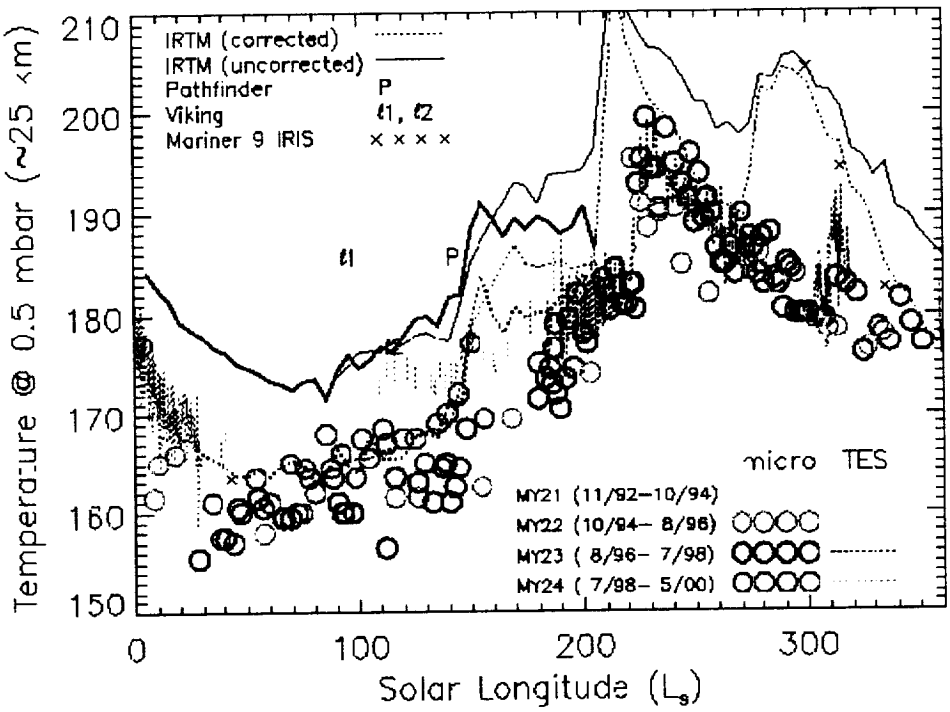

Plate 1. A comparison of Mars measurements for low- to midlatitude atmospheric temperatures at the 0.5 mbar pressure level, as a function of Mars solar longitude L_S. The 1992-1999 millimeter and 1997-1999 TES measurements are color coded to distinguish interannual variability, and we apply an arbitrary numbering of Mars years (year 1 beginning April 11, 1955) to specify the interannual relationships among the Viking (MY12-13), Pathfinder (MY23), MGS TES (MY23-24), Mariner 9 IRIS (MY9-10), and millimeter measurements (MY21-24). The localized entry measurements by Viking [*Seiff and Kirk*, 1977] and Pathfinder [*Schofield et al.*, 1998] are represented by letter symbols (P, *l*1, *l*2). The dayside average IRTM 15 μm temperatures for three years of the Viking IRTM observations are represented by the dashed line (uncorrected, [*Kieffer et al.*, 1977], year 12 thin line, year 13 thick line). These dayside IRTM temperatures may be biased 10-15 K warm, owing to strong contamination from surface emission. The dotted lines (corrected) reflect the decrease in the 15 μm IRTM temperatures, resulting from the *Wilson and Richardson* [2000] reanalysis. Mariner 9 IRIS measurements are presented by crosses [*Conrath*, 1975].

fall 15 K above the temperatures retrieved by the millimeter measurements in essentially all seasons. By comparison, the corrected IRTM temperatures (dotted lines) are reasonably consistent (within 5 K) with the seasonal and interannual dependence of Mars atmospheric temperatures displayed by the millimeter measurements. Within the millimeter data set, interannual variations in global average atmospheric temperatures (by 5-15 K) are most prominent during the perihelion dust storm season (L_S =200°-340°) and during the northern summer/fall period (L_S=100°-200°). These are the same seasons in which millimeter and corrected IRTM temperatures exhibit their largest differences.

The general character of the perihelion dust storm activity is very similar in the consecutive years 22 and 23. An increase in global atmospheric temperatures occurred around L_S=220° in 1995 (year 22), which is very similar to the 1997 (year 23) L_S=225° Noachis Terra event in terms of atmospheric temperature changes. A second, weaker event also occurred at L_S=270° in 1995 (year 22), suggesting that multiple dust storms in a perihelion season may be typical behavior. However, dust storm activity appears to have persisted later in the season in year 23 versus year 22, creating a 5-10 K warmer global atmosphere over L_S=310°-340° in year 23. Perihelion temperature increases were also observed in the two previous Mars years 20 (not shown in Plate 1) and 21. The L_S at which these events initiated are not determined by the limited frequency of the measurements (particularly in year 20), but the year 21 event appears to have occurred shortly before L_S=250°, on the basis of peak temperatures observed at L_S=254° in 1994. This would be substantially later in season than the L_S=225° storms of years 22 and 23, but earlier in season than the initiation of the 1977b dust storm in year 12. Peak atmospheric temperatures observed during the year 21 dust event were actually 10 K greater than observed in years 22 and 23 and comparable to the atmospheric temperature increases that accompanied the Mariner 9 (year 9) and Viking (year 12) great dust storms. (Figure 6 includes five 1994 dust storm observations which were obtained by Emannuel Lellouch with the 30 m IRAM telescope at Pico Veleta, Spain.) The extended record of atmospheric pressure from the Viking landers suggests weaker perihelion dust storms, comparable to those of the 1990s, occurred in years 13 and 14, whereas a significantly stronger perihelion storm occurred in year 15 [*Tillman*, 1985; *Leovy et al.*, 1985).

Perihelion atmospheric temperatures may exhibit two distinct cases, corresponding to great dust storms and regional dust storms. Both cases show global atmospheric temperature increases, but those corresponding to regional dust storms are roughly half as large as those corresponding to global dust storms. As a rough estimate of their relative frequency, we note that for the nine perihelion dust storms measured by spacecraft or millimeter observations, four of these could be classified as great or planet encircling storms (40-50% frequency, similar to the suggestions of *Zurek and Martin*, [1993]). On the other hand, the brevity, discontinuous coverage, and poor sampling of the observational record do not rule out a continuous range of perihelion dust storm activity over time. In either case, the millimeter measurements of atmospheric temperature increases during regional dust storms in the past 4 Mars years suggest that perihelion dust storms of regional or greater extent occur in every Mars year (in accord with the suggestion of *Zurek*, [1982]).

Outside of the perihelion dust storm season, differences among the corrected IRTM, millimeter, and TES measurements, and variability within the millimeter temperatures are most prominent during the northern summer/fall seasons (L_S=100°-200°). For example, TES temperatures exhibit peak differences (5 K) with contemporaneous millimeter measurements over L_S=120°-140° in 1999 (although ~1 K of this difference is associated with low- to high-latitude temperature gradients weighted in the disk-averaged millimeter observations). This period also corresponds to the 10-20 K disagreements between the millimeter-TES profiles and the Viking-Pathfinder descent measurements of atmospheric temperature (as well as the unusual Pathfinder temperature inversion near the 2 mbar, 10 km altitude level). Part of these differences probably reflects increased spatial and temporal variability of the Mars atmosphere in this season. The multiyear millimeter observations show a distinct increase in short-term

and interannual variability beyond L_S ~90°. For example, the lower 10-20 km of the Mars atmosphere was 5-10 K warmer in year 22 than in year 23 over L_S=115°-200° [*Clancy*, 1996], and year 23 was 5-10 K warmer than years 21 and 22 at L_S=200°. In fact, 1999 (year 24) millimeter measurements indicate a distinct rise in global atmospheric temperatures over L_S=100°-150°, that place them 5 K warmer than in years 22 and 23, but in close agreement with the corrected IRTM temperatures for this northern summer season. TES temperature measurements at L_S=180°-190° in 1997 versus 1999 also indicate 5 K warmer temperatures in Mars year 24 versus 23. In addition, variations among the millimeter, TES, and Viking IRTM (corrected) temperatures show a distinct maximum of 10-15 K over L_S=150°-180° in this northern summer/fall season.

The cold aphelion period (L_S=10°-90°) presents the greatest degree of repeatability in Mars atmospheric temperatures, in terms of variability within the long-term millimeter data set and in comparison between the corrected IRTM and millimeter observations. Millimeter observations of aphelion atmospheric temperatures exist for years 14, 15, and 19-24. When corrected for the 3-4 K effects of high northern latitude weighting (see discussion of Figure 5), these millimeter temperatures exhibit excellent agreement with TES, MGS and Viking radio occultation, and corrected Viking IRTM 15 μm measurements. On this basis, all 11 observed Mars aphelions over the period year 9 to year 24, including the Mariner 9 period, have exhibited comparably cold atmospheric temperatures (to within 5 K) at this altitude level.

4. Related Changes in Dust Loading

To a large degree, the amount of dust suspended in the thin CO_2 atmosphere determines the average profile of Mars atmospheric temperatures. The direct effects of dust aerosols on the thermal profile of the Mars atmosphere include atmospheric heating due to absorption of solar flux and atmospheric cooling and heating associated with broadband thermal infrared emission and absorption [e.g., *Pollack et al.*, 1979; *Zurek*, 1978]. Regional dust storms force abrupt 10-30 K increases in global atmospheric temperatures to altitudes well above 50 km [*Clancy et al.*, 1994]. Mariner 9 Infrared Interferometric Spectrometer (IRIS) observations [*Hanel et al.*, 1972] of elevated Mars atmospheric temperatures during the 1971 global dust storm form the basis for much of our current understanding of atmospheric dust-temperature relationships on Mars [*Gierasch and Goody*, 1972; *Conrath*, 1975] (review by *Kahn et al.*, [1992]). Analysis of the Viking lander descent temperature profiles and visible dust column opacities explored a broader range of opacity and diurnal conditions, and provided observational constraints on the solar absorption properties of the dust [*Pollack et al.*, 1979]. Viking IRTM 15 μm data were instrumental in defining the visible/IR opacity ratio of the dust, which relates the relative efficiencies of solar absorption-heating and thermal-emission cooling by the dust [*Zurek*, 1982; *Martin*, 1986; *Clancy et al.*, 1995].

There remain considerable uncertainties in the temperature forcing of the Mars atmosphere as a result of dust loading. Reanalysis of the Viking measurements and new Pathfinder measurements indicate that the dust absorbs solar flux less efficiently (compare solar band average single scattering albedo = 0.86 [*Pollack et al.*, 1979] versus 0.92 [*Clancy and Lee*, 1991] versus 0.88 [*Ockert-Bell et al.*, 1997] versus 0.90 [*Tomasko et al.*, 1999]) and that mean dust particle sizes are ~50% smaller than indicated in the *Toon et al.* [1977] Mariner 9 based dust model [*Chassefière et al.*, 1995; *Clancy et al.*, 1995; *Pollack et al.*, 1995; *Tomasko et al.*, 1999]. In addition, very little is known about the temporal and spatial variations of the dust particle sizes and absorbing properties. Analysis of column-integrated dust scattering observations from the 1997 Pathfinder lander indicates that local dust particle sizes and solar absorption properties are remarkably similar to those determined from reanalysis of the 1977 Viking lander observations [*Tomasko et al.*, 1999]. However, these surface-based measurements relate

to similar locales (northern low-latitude basins) and to dust properties in the lower atmosphere. Dust sizes, and so their emission/absorption properties, are almost certain to vary with latitude and altitude, owing to size-dependent dust-settling rates [e.g., *Murphy et al.*, 1990].

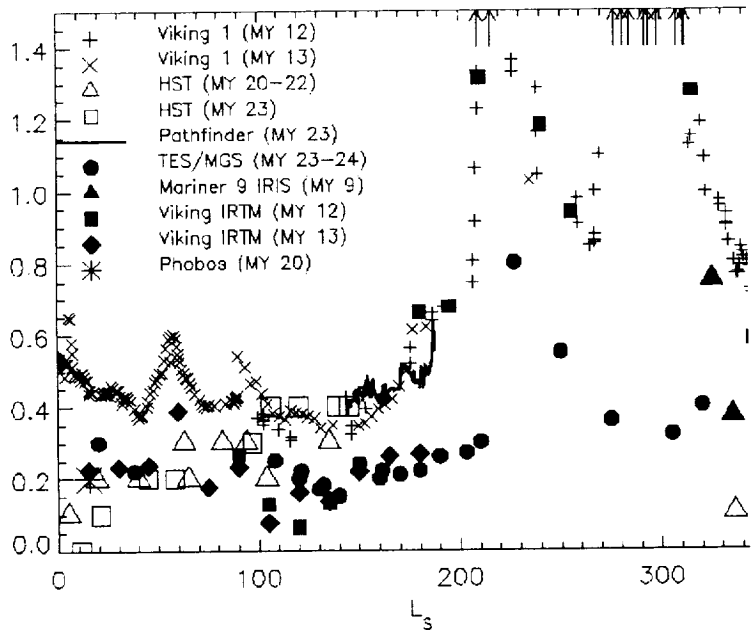

Figure 10. A comparison of visible dust column opacities at Mars northern low latitudes, as determined from 1971-1972 Mariner 9 IRIS (solid triangles) (scaled from 9 μm opacity [*Fenton et al.*, 1997]), 1976-1978 Viking 1 lander (plus symbols in year 12, cross symbols in year 13) [*Colburn et al.*, 1989], 1976-1978 Viking IRTM (solid squares in year 12, solid diamonds in year 13) (scaled from 9 μm opacity [*Martin*, 1986]), 1989 Phobos (asterisk) [*Chassefière et al.*, 1992; *Moroz et al.*, 1991], 1997 Pathfinder (solid line) [*Smith and Lemmon*, 1999], 1997-1998 MGS TES (solid circles) [*Smith et al.*, this issue], and 1995-1997 HST (open triangles in years 20-22, open squares in year 23) [*Wolff et al.*, 1999; *Clancy et al.*, 1999] measurements. The Viking lander opacities include only PM observations and have been smoothed with a five-point running mean. Arrows indicate opacities greater than 2 for Viking lander measurements during the 1977a and 1977b dust storms. The 1997-1998 TES and 1972 IRIS values are determined from 9 μm opacity measurements, which have been scaled by a factor of 2 to obtain equivalent visible dust opacities.

Perhaps most surprising is how little we understand about the average behavior of Mars atmospheric dust loading, including its seasonal and interannual variability. The generally held model of dust loading for the global Mars atmosphere is drawn largely from the Viking lander measurements of column dust opacities, which implied a minimum background dust opacity of ~0.5 [*Pollack et al.*, 1979; *Colburn et al.*, 1989]. Such dusty conditions were viewed as consistent with the warm atmospheric temperatures determined from the Viking descent measurements and the uncorrected IRTM 15 μm data [e.g., *Pollack et al.*, 1979; *Haberle et al.*, 1997; *Forget et al.*, 1999]. The 1997 Pathfinder measurements of dust opacity and atmospheric temperatures have been interpreted as verification of this dusty, warm model and its long-term applicability [*Schofield et al.*, 1998; *Haberle et al.*, 1999; *Smith and Lemmon*, 1999]. The colder atmospheric temperatures returned from the long-term record of millimeter observations [*Clancy et al.*, 1996] and their agreement with the presented 1997-1998 TES and millimeter

measurements represent a significant contradiction to this Viking-based climatology. If the 1988-1998 Mars atmosphere is 15 K cooler than at the time of the Viking period (1976-1979), it implies that the average dust loading of the global Mars atmosphere is significantly smaller now than at the time of the Viking period [*Clancy et al.*, 1990, 1996]. Dust-dependent temperature profile calculations from Mars global circulation models [*Wilson and Hamilton*, 1996; *Haberle et al.*, 1997] suggest that that global dust loading levels over the entire Mars year must decrease by at least a factor of 2 between these periods to produce such colder atmospheric temperatures. TES nadir dust opacity retrievals in the 9 μm silicate absorption band provide a valuable test for determining whether such large changes in atmospheric dust loading have occurred between the late 1970s and the 1990s.

Figure 10 presents a comparison of visible dust column opacities at 0°-30° N latitudes as derived from Mariner 9 IRIS (solid triangles) 9 μm dust opacities (1972, scaled by a factor of 2 [*Fenton et al.*, 1997]); Viking lander 1 (plus signs in year 12, crosses in year 13) solar extinction measurements (1976-1978 [*Colburn et al.*, 1989]); Viking IRTM (solid squares in year 12, solid diamonds in year 13); 9 μm dust opacities (1976-78, scaled by a factor of 2 [*Martin*, 1986]; the colder atmospheric temperatures determined by the Wilson and Richardson reanalysis of IRTM 15 μm radiances will affect the 9 μm dust opacities retrieved from IRTM observations only slightly, reducing retrieved dust opacities by 10-20%); 1989 Phobos (asterisk) solar occultation [*Chassefière et al.*, 1992] and spectroscopic [*Drossart et al.*, 1991; *Moroz et al.*, 1991) observations; 1995-1997 Hubble Space Telescope (HST) (open triangles in years 20-22, open squares in year 23) imaging [*James et al.*, 1994; *Wolff et al.*, 1999] and spectroscopy [*Clancy et al.*, 1999]; and Pathfinder solar extinction imaging (solid line [*Smith et al.*, 1997]). Included in Figure 10 are the average TES 9 μm dust opacities for the 0°-30° N latitude range in 1997-1998 (solid circles) [*Smith et al.*, this issue], which have been scaled by a factor of 2 to present comparable visible dust opacities [*Zurek*, 1982; *Clancy et al.*, 1995]. Afternoon dust opacities from the Viking 1 lander record (smoothed with a running five-point average) are presented, and the Viking and Pathfinder opacities are scaled to a surface pressure of 6.1 mbar (in accord with the TES opacities).

Several points follow from the comparisons of Figure 10. The Mars southern spring/summer atmosphere in 1996-1998 (years 22-23) does show significantly lower dust loading than during the 1976-1977 Viking period (year 12). At L_S of 190°-320° the 1997-1998 TES measurements imply visible dust opacities at northern low latitudes which are 2-8 times lower than during the Viking period. TES dust measurements prior to the Noachis Terra storm show a factor of 2-3 less dust loading, compared to Viking 1 lander and IRTM measurements prior to the 1977a storm (0.3 versus 0.6-0.8 at L_S=180°-205°. Notice, however, that IRTM dust opacities at L_S=180°-185° are lower in year 13 than in year 12). Perihelion dust storm activity (L_S=205°-280°) was much weaker in 1997-1998 relative to the 1977 period. The Noachis Terra dust storm of 1997 led to relatively modest dust loading in the northern hemisphere, as compared to the large dust opacities observed by both Viking landers and IRTM during the 1977a and 1977b dust storms (visible dust opacities of 0.6-0.8 versus 2-4). Although there are 30-50% increases in TES dust opacities between L_S=300° and 360° (which correspond to distinct L_S=310° and 340° atmospheric heating events; see Figure 5), there was no second dust storm in 1997-1998 comparable to the 1977b storm. Consequently, the L_S=280°-320° seasonal range was also much less dusty (3-8 times) in year 23 than during the equivalent season in year 12. This seasonal range was also less dusty in 1998 than observed after the 1971 great dust storm (year 9; compare TES and IRIS), although by L_S=330°-340° the 1972 dust loading had decayed to comparable levels observed in 1998.

The L_S=350°-180° period of northern spring/summer exhibits a more complex variation among the TES, Viking lander and IRTM, HST, and Phobos dust opacity measurements. At L_S=360° TES measurements are 2-3 times larger than the HST opacities, but are in reasonable agreement with the dust columns measured by Viking 1 and IRTM in 1977. However, the L_S=300°-360° period in 1998

presents an increasing dust column owing to the late season dust storm events at L_S=310° and 340° (Figure 5). By comparison, the Viking 1977 and Mariner 9 1972 dust opacities over this L_S range decreased by a factor of 2-4, associated with the decay of the 1977b and 1971 storms. The TES opacities at L_S=20°-40° are comparable to the Phobos (year 20), HST (Years 20-23), and Viking IRTM (years 12-13) measurements for this season (τ_{vis} ~0.1-0.3), and are roughly a factor of 2 less than the Viking lander 1 opacities. The northern summer season at L_S=100°-180° shows good agreement among the Viking lander, HST, and Pathfinder observations, whereas the Viking IRTM (1976, 1978) and MGS TES (1997, 1999) measurements are typically lower by a factor of 2.

The differences between the 1978 Viking lander and IRTM opacities over L_S=10°-180° (year 13) and the 1997 TES and Pathfinder measurements at L_S=190° (year 23) are particularly surprising, as these are contemporaneous measurement sets. *Zurek* [1982] raised the possibility that Viking lander dust opacities obtained prior to the 1977 storms may not be fully representative of low- to midlatitude dust loading at this time. We suggest that the Viking and Pathfinder lander opacities over L_S=10°-190° include the effects of enhanced boundary layer dust loading from dust devil activity in these low basins [e.g., *Metzger et al.*, 1999], as well as contributions from afternoon cloud opacities (particularly for the L_S=60°-140° aphelion cloud period). Incomplete separation of cloud versus dust scattering is the major uncertainty in determining HST dust opacity, as ice particle scattering is 3-4 times more effective than dust scattering for increasing the visible/ultraviolet brightnesses analyzed in these studies [*Wolff et al.*, 1999; *Clancy et al.*, 1999]. The recent identification of the aphelion cloud belt in Viking IRTM observations [*Tamppari et al.*, 1999] implies that water ice clouds may affect the aphelion dust opacities retrieved from Viking lander [*Colburn et al.*, 1989] and orbiter [*Thorpe*, 1981] analyses. Unaccounted effects from cloud opacities and lower boundary enhancements of dust loading both tend to bias the Viking lander opacities high relative to the vertically-extended, dust-only opacities retrieved from 9 μm TES and IRTM nadir retrievals. Such a change to the Viking-based characterization of dust loading in this season is at least partly corroborated by the lower atmospheric temperatures determined for this season in 1976 and 1978 (years 12 and 13) by the *Wilson and Richardson* [2000] reanalysis of the Viking IRTM 15 μm measurements.

The dust opacity measurements of Figure 10 indicate decreased atmospheric dust columns between the Viking and recent periods, particularly for the L_S=190°-340° seasonal range. The decreased dust loading during the perihelion dust storm season in 1997-1998 also corresponds to significantly colder atmospheric temperatures (by 10-15 K) in 1997-1998 versus 1977. On the other hand, 10-15 K differences between the millimeter and Viking 15 μm temperatures (corrected) over L_S=150°-180° correspond to a seasonal range in which HST, Viking, and Pathfinder dust column measurements exhibit relatively good agreement, and Viking IRTM opacities are actually a factor of 2 lower. The abrupt 10-15 K increases in Viking 15 μm IRTM and millimeter temperatures over L_S=145°-150° in years 12 and 13 were not accompanied by comparably sharp increases in the atmospheric dust column, as evidenced by either the Viking lander or Viking IRTM opacity records.

It is also notable that the corrected 15 μm IRTM measurements of 20-30 km atmospheric temperatures are now in conflict with the two Viking descent temperature profiles at L_S=96° and 117°. A similar conflict exists between the cold millimeter profiles and the warm Pathfinder descent temperature profile at L_S=143° in 1997 [*Schofield et al.*, 1998; *Clancy and Sandor*, 1998, Figure 8]. The millimeter temperature measurements do show distinctive interannual and short-term (over 1-2 weeks) variability during this period. Although there is no clear correlation of dust opacity variations with these temperature differences, a significant dust storm did erupt in Valles Marineris several days before and nearby the Pathfinder landing site on Mars [*Wolff et al.*, 1999]. This storm was observed to decay shortly after the Pathfinder landing, and so may have contributed to regionally and temporally restricted dust loading at the time of the Pathfinder entry.

At this time, a simple relationship between Mars global-average atmospheric temperatures and dust column opacities is not evident. The Viking-based model of a constant background dust level, which is well mixed vertically and horizontally (over low- to midlatitudes) implies a fairly direct relationship between warmer atmospheric temperatures and increased dust column opacities. This behavior appears to be present during the perihelion dust storm season (L_S=205°-360°), where colder temperatures and lower dust column opacities are unambiguously presented in 1997-1998. However, such a direct relationship is not evident during the L_S=0°-200° seasonal range, where descent temperature profiles disagree with global remote sensing measurements; interannual dust opacity variations may or may not exist, depending on whether Viking lander or IRTM 9 μm measurements best characterize global dust loading during 1976-1978.

It has been argued that the influence of nonlinear interactions between water ice and dust aerosols may serve to enhance short-term, interannual, and spatial (e.g., the descent profiles represent transitory local conditions) variations of atmospheric dust loading and enforce the confinement of solar heating by dust aerosols to altitudes below 10-15 km in the northern spring/summer seasons [*Clancy et al.*, 1996]. Recent modeling of this mechanism suggests the potential importance of ice condensation on dust aerosols, in terms of both gravitational settling rates and the aerosol single scattering albedo [*Rodin et al.*, 1999]. The cold Mars atmosphere around aphelion implies low altitudes ($\leq$10 km) for water ice cloud formation during the northern spring/summer seasons. The abrupt rise in Mars atmospheric temperatures in late northern summer (over L_S=140°-150°) may reflect a discrete increase in dust heating of the atmosphere, as cloud formation and its suppression of dust solar absorption break down in late northern summer. Limb profiling of atmospheric temperatures, dust, and clouds by TES will address these questions shortly.

5. Conclusions

Extensive temperature profiling measurements of the Mars atmosphere were obtained by spacecraft infrared (MGS/TES) and ground-based millimeter (Kitt Peak NRAO) experiments during the 1997-1999 aerobraking and early mapping phases of the MGS mission. Appropriate latitude averages of the spatially resolved MGS temperatures are compared to the disk-averaged millimeter temperatures for the 0-30 km altitude region of the Mars atmosphere. These profile comparisons demonstrate 2-5 K agreement between the TES and millimeter data sets for selected L_S of 205°-214°, 226°-227° (the Noachis Terra regional dust storm), 300°-308°, 28°-34°, 108°-112° (Viking descent profile comparison), and 141°-144° (Pathfinder descent comparison). In addition, 1999 MGS and 1978 Viking radio occultation measurements exhibit good agreement with a 1999 millimeter temperature profile for L_S=74°-77°. Time sequences of TES and millimeter temperatures at pressure levels of 0.3 mbar (~30 km altitude) and 0.5 mbar (~25 km altitude) are presented over the extended September 1997 (L_S=190°) to September 1999 (L_S=180°) period. Both data sets show a series of very abrupt global atmospheric temperature increases of 5-15 K, the largest of which is related to the late November 1997 Noachis Terra regional dust storm [*Christensen et al.*, 1998; *Smith et al.*, this issue]. Comparison of the 1997-1999 millimeter observations to previous years of millimeter observations indicates very similar seasonal and dust storm behaviors for the Mars atmosphere over the past 4-5 Mars years, including abrupt 10-15 K global temperature increases in each Mars perihelion season.

Over the entire 1997-1999 period of observations, global Mars atmospheric temperatures determined from the TES and millimeter measurements are 10-20 K colder than have been inferred from Viking [e.g., *Haberle et al.*, 1997] and Pathfinder [e.g., *Schofield et al.*, 1998] atmospheric measurements. These differences are substantially reduced by the *Wilson and Richardson* [2000] reanalysis of the Viking 15 μm radiances, which leads to decreases of 5-15 K in 0.5 mbar atmospheric temperatures derived for

the Viking period. On the basis of this correction, the Mars atmosphere during 1997-1999 is ~5-10 K colder than during the 1976-1978 Viking period for the seasonal range L_S=150°-180°, 10-15 K colder over L_S=205°-330°, but within 5 K of the Viking period temperatures for the remainder of the Mars year.

Colder current conditions over the L_S=205°-330° period correlate with relatively low perihelion dust loading in 1997-98 as compared to 1977. Dust opacities retrieved from the 1997-1998 TES 9 μm absorption measurements are 2-8 times smaller than those determined from Viking lander and IRTM observations over this perihelion dust storm season. Away from the perihelion southern summer season, interannual variations in global atmospheric temperatures are more modest and are not clearly associated with distinct changes in column dust opacities. Global average 0.5 mbar temperatures from millimeter and TES measurements are 5-10 K warmer during early northern summer (L_S=100°-150°) in 1998-1999 (year 24) versus 1993-1997 (years 21-23), and 5-10 K colder during late northern summer (L_S=150°-180°) versus 1976-1978 (years 12 and 13). Changes in the vertical distribution rather than the vertical column of dust loading may be responsible for these interannual variations in northern summer atmospheric temperatures. The Mars aphelion atmosphere (northern spring, L_S=0°-100°) presents minimum conditions of interannual and short-term variability. Minimum dust opacities (τ_{vis} ~0.1-0.3), peak cloud opacities (τ_{vis} ~0.1-0.5), and cold atmospheric temperatures would be typical of all observed Mars aphelion seasons if Viking IRTM 15 and 9 μm measurements rather than the Viking lander measurements are representative of 1976-1978 global conditions for Mars atmospheric temperatures and dust loading in this season.

These results conflict with the conclusions from Pathfinder atmospheric analyses [*Smith and Lemmon*, 1999; *Haberle et al.*, 1999; *Magalhães et al.*, 1999) that the Mars atmosphere has remained in the dusty, warm state characterized by Viking lander measurements since the time of these Viking observations 20 years ago. They lend support to conclusions that water ice clouds are likely to form at lower altitudes than previously thought (below 10 km around aphelion), and may contribute significant influences on the photochemistry, dust radiative forcing, and interannual variability in the global Mars climate system [*Clancy et al.*, 1996].

Acknowledgments. This work presents a set of millimeter-wave observations which were obtained and analyzed under JPL contract 960349 as part of a broad program of science advisory support for the Mars Global Surveyor aerobraking operations. We acknowledge the privilege and opportunity of our participation in the MGS Atmospheric Advisory Group and the personal support extended by Dan Lyons and Richard Zurek. The TES measurements employed in this comparison result from the diligent efforts of the entire TES team and the joint JPL/Lockheed Martin spacecraft operations. Observational support for the Kitt Peak millimeter measurements was graciously and generously provided by the National Radio Astronomy Observatory (NRAO, operated by Associated Universities, Inc., under cooperative agreement with the National Science Foundation). We are especially indebted to the Kitt Peak 12 m NRAO telescope operators.

References

Chassefière, E., J. E. Blamont, V. A. Krasnopolsky, O. I. Korablev, S. K. Atreya, and R. A. West, Vertical structure and size distributions of Martian aerosols from solar occultation measurements, *Icarus, 100*, 48-59, 1992.

Chassefière, E., P. Drossart, and O. Korablev, Post-Phobos model for the altitude and size distribution of dust in the low Martian atmosphere, *J. Geophys. Res., 100*, 5525-5540, 1995.

Christensen, P. R. et al., Thermal emission spectrometer experiment: Mars Observer mission, *J. Geophys. Res., 97*, 7719-7734, 1992.

Christensen, P. R. et al., Results from the Mars Global Surveyor thermal emission spectrometer investigation, *Science, 279*, 1692-1698, 1998.

Clancy, R. T., Atmospheric dust-water ice interactions: Do they play important roles in the current Mars climate?, in Workshop on Evolution of Martian Volatiles, *LPI Tech. Rep. 96-01*, p. 9, Lunar and Planet. Sci., Houston, Tex., 1996.

Clancy, R. T., and S. W. Lee, A new look at dust and clouds in the Mars atmosphere: Analysis of emission-phase-function sequences from global Viking IRTM observations, *Icarus, 93*, 135-158, 1991.

Clancy, R. T., and H. Nair, Annual (perihelion-aphelion) cycles in the photochemical behavior of the global Mars atmosphere, *J. Geophys. Res., 101*, 12,785-12,790, 1996.

Clancy, R. T., and B. J. Sandor, CO_2 ice clouds in the upper atmosphere of Mars, *Geophys. Res. Lett.*, 25, 489-492, 1998.

Clancy, R. T., D. O. Muhleman, and B. M. Jakosky, Variability of carbon monoxide in the Mars atmosphere, *Icarus, 55*, 282-301, 1983.

Clancy, R. T., D. O. Muhleman, and G. L. Berge, Global changes in the 0-70 km thermal structure of the Mars atmosphere derived from 1975-1989 microwave CO spectra, *J. Geophys. Res., 95*, 14543-14,554, 1990.

Clancy, R. T., E. Lellouch, Y. N. Billawala, B. J. Sandor, and D. J. Rudy, Microwave observations of a 1994 Mars global dust storm, *Bull. Am. Astron. Soc., 26*, 1130, 1994.

Clancy, R. T., S. W. Lee, G. R. Gladstone, W. McMillan, and T. Roush, A new model for Mars atmospheric dust based upon analysis of ultraviolet through infrared observations from Mariner 9, Viking, and Phobos, *J. Geophys. Res., 100*, 5251-5263, 1995.

Clancy, R. T., A. W. Grossman, M. J. Wolff, P. B. James, Y. N. Billawala, B. J. Sandor, S. W. Lee, and D.J. Rudy, Water vapor saturation at low altitudes around Mars aphelion: A key to Mars climate?, *Icarus, 122*, 36-62, 1996.

Clancy, R. T., M. J. Wolff, and P. B. James, Minimal aerosol loading and global increases in atmospheric ozone during the 1996-1997 Martian northern spring season, *Icarus, 138*, 49-63, 1999.

Colaprete, A., O. B. Toon, and J. A. Magalhães, Cloud formation under Mars Pathfinder conditions, *J. Geophys. Res., 104*, 9043-9054, 1999.

Colburn, D. S., J. B. Pollack, and R. M. Haberle, Diurnal variations in optical depth at Mars, *Icarus, 79*, 159-189, 1989.

Conrath, B. J., Thermal structure of the Martian atmosphere during the dissipation of the dust storm of 1971, *Icarus, 24*, 36-46, 1975.

Conrath, B. J., J. C. Pearl, M. D. Smith, W. C. Maguire, S. Dason, M. S. Kaelbererr, and P. R. Christensen, Mars Global Surveyor Thermal Emission Spectrometer (TES) observations: Atmospheric temperatures during aerobraking and science phasing, *J. Geophys. Res.*, this issue.

Drossart, P., J. Rosenqvist, S. Erard, Y. Langevin, J. P. Bibring, and M. Combes, Martian aerosol properties from the Phobos/ISM experiment, *Ann. Geophys., 9*, 754-760, 1991.

Fenton, L., J. C. Pearl, and T. Z. Martin, Mapping Mariner 9 dust opacities, *Icarus, 130*, 115-124, 1997.

Forget, F., F. Hourdin, R. Fournier, C. Hourdin, O. Talagrand, M. Collins, S. R. Lewis, P. L. Read, and J-P. Huot, Improved general circulation models of the Martian atmosphere from the surface to above 80 km, *J. Geophys. Res., 104*, 24,155-24,175, 1999.

Gierasch, P. J., and R. M. Goody, The effect of dust on the temperature of the Mars atmosphere, *J. Atmos. Sci., 29*, 400-402, 1972.

Haberle, R. M., J. B. Pollack, J. R. Barnes, R. W. Zurek, C. B. Leovy, J. R. Murphy, H. Lee, and J. Schaeffer,

Mars atmospheric dynamics as simulated by the NASA Ames General Circulation Model, 1. The zonal-mean circulation, *J. Geophys. Res., 98*, 3093-3123, 1993.

Haberle, R. M., J. R. Barnes, J. R. Murphy, M. M. Joshi, and J. Schaeffer, Meteorological predictions for the Mars Pathfinder lander, *J. Geophys. Res., 102*, 13,301-13,311, 1997.

Haberle, R. M., M. M. Joshi, J. M. Murphy, J. R. Barnes, J. T. Schofield, G. Wilson, M. Lopez-Valverde, J. L. Hollingsworth, A. F. C. Bridger, and J. Schaeffer, General circulation model simulations of the Mars Pathfinder atmospheric structure investigation/meteorology data, *J. Geophys. Res., 104*, 8957-8974, 1999.

Hanel, R. A., et al., Investigation of the Martian environment by infrared spectroscopy on Mariner 9, *Icarus, 17*, 423-442, 1972.

Hinson, D. P., R. A. Simpson, J. D. Twicker, G. L. Tyler, and F. M. Flasar, Initial results from radio occulatation measurements with Mars Global Surveyor, *J. Geophys. Res., 104*, 26,997-27,102, 1999.

James, P. B., R. T. Clancy, S. W. Lee, L. J. Martin, R. B. Singer, E. Smith, R. A. Kahn, and R. W. Zurek, Monitoring Mars with the Hubble Space Telescope: 1990-1991 observations, *Icarus, 109*, 79-101, 1994

Kahn, R. A., T. Z. Martin, R. W. Zurek, and S. W. Lee, The Martian dust cycles, in *Mars*, edited by H. H. Kieffer et al., pp. 1017-1053, Univ. of Ariz. Press, Tucson, 1992.

Keating, G. M., et al., The structure of the upper atmosphere of Mars: In situ accelerometer measurements from Mars Global Surveyor, *Science, 279*, 1672-1676, 1998.

Kieffer, H. H., S. C. Chase, E. D. Miner, F. D. Palluconi, G. Munch, G. Neugebauer, and T. Z. Martin, Infrared thermal mapping of the Martian surface and atmosphere: First results, *Science, 193*, 780-786, 1976.

Kieffer, H. H., T. Z. Martin, A. R. Peterfreund, B. M. Jakosky, E. D. Miner, and F. D. Palluconi, Thermal and albedo mapping of Mars during the Viking primary mission, *J. Geophys. Res., 82*, 4249-4291, 1977.

Leovy, C. B., J. E. Tillman, W. R. Guest, and J. R. Barnes, Interannual variability of Martian weather, in *Recent Advances in Planetary Meteorology*, edited by G. E. Hunt, pp. 69-84, Cambridge Univ. Press, New York, 1985.

Lindal, G. F., H. B. Hotz, D. N. Sweetnam, Z. Shippony, J. P. Brenkle, G. V. Hartsell, R. T. Spear, and W. H. Michael, Jr., Viking radio occultation measurements of the atmosphere and topography of Mars: Data acquired during 1 Martian year of tracking, *J. Geophys. Res., 84*, 8443-8456, 1979.

Magalhães, J. A., J. T. Schofield, and A. Seiff, Results of the Mars Pathfinder atmospheric structure investigation, *J. Geophys. Res., 104*, 8943-8956, 1999.

Martin, T. Z., Mean thermal and albedo behavior of the Mars surface and atmosphere over a Martian year, *Icarus, 45*, 427-446, 1981.

Martin, T. Z., Thermal infrared opacity of the Mars atmosphere, *Icarus, 66*, 2-21, 1986.

Metzger, S. M., J. R. Carr, J. R. Johnson, T. J. Parker, and M. T. Lemmon, Dust devil vortices seen by the Mars Pathfinder camera, *Geophys. Res. Lett.*, 26, 2781-2784, 1999.

Moroz, V. I., et al., Characteristics of aerosol phenonmena in martian atmosphere from KRFM experiment data, *Planet. Space Sci., 39*, 199-208, 1991.

Murphy, J. R., O. B. Toon, R. M. Haberle, and J. B. Pollack, Numerical simulations of the decay of Martian global dust storms, *J. Geophys. Res., 95*, 14629-14648, 1990.

Ockert-Bell, M. E., J. F. Bell III, J. B. Pollack, C. P. McKay, and F. Forget, Absorption and scattering properties of the martian dust in the solar wavelengths, *J. Geophys. Res., 102*, 9039-9050, 1997.

Pollack, J., D. Colburn, F. M. Flasar, R. Kahn, C. E. Carlston, and D. C. Pidek, Properties and effects of dust particles suspended in the Mars atmosphere, *J. Geophys. Res., 84*, 2929-2945, 1979.

Pollack, J. B., M. E. Ockert-Bell, and M. K. Shepard, Viking lander image analysis of Martian atmospheric dust, *J. Geophys. Res., 100*, 5235-5250, 1995.

Richardson, M. I., Comparison of microwave and infrared measurements of Martian atmospheric temperatures: Implications for short-term climate variability, *J. Geophys. Res.*, 103, 5911-5918, 1998.

Rodin, A. V., R. T. Clancy, and R. J. Wilson. Dynamical Properties of Mars water ice clouds and their interactions with atmospheric dust and radiation, *Adv. Space Res., 23*, 1577-1585, 1999.

Schofield, J. T., J. R. Barnes, D. Crisp, R. M. Haberle, S. Larsen, J. A. Magalhães, J. R. Murphy, A. Seiff, and G. Wilson, The Mars Pathfinder atmospheric structure investigation/meteorology (ASI/MET)

experiment, *Science, 278*, 1752-1758, 1997.

Seiff, A. and D. B. Kirk, Structure of the atmosphere of Mars in summer mid-latitudes, *J. Geophys. Res., 82*, 4364-4378, 1977.

Smith, M. D., B. J. Conrath, J. C. Pearl, and P. R. Christensen, Mars Global Surveyor Thermal Emission Spectrometer (TES) observations of dust opacity during aerobraking and science phasing, *J. Geophys. Res.*, this issue.

Smith, P. H., and M. Lemmon, Opacity of the Martian atmosphere measured by the Imager for Mars Pathfinder, *J. Geophys. Res., 104*, 8975-8986, 1999.

Smith, P. H., et al., Results from the Mars Pathfinder camera, *Science, 278*, 1758-1768, 1997.

Tamppari, L. K., R. W. Zurek, and D. A. Paige, Viking era water ice clouds, *J. Geophys. Res.*, this issue.

Thorpe, T. E., Mars opacity effects observed in the northern hemisphere by Viking Orbiter imaging, *J. Geophys. Res., 86*, 11419-11429, 1981.

Tillman, J. E., Martian meteorology and dust storms from Viking observations, in *Case for Mars II*, edited by C.P. McKay, pp. 333-342, Univelt, San Diego, Calif., 1985.

Titov, D. V., W. J. Markiewicz, N. Thomas, H. U. Keller, R. M. Sablotny, M. G. Tomasko, M. T. Lemmon, and P. H. Smith, Measurements of atmospheric water vapor on Mars by the Imager for Mars Pathfinder, *J. Geophys. Res., 104*, 9019-9026, 1999.

Tomasko, M. G., L. R. Doose, E. Wegryn, and P. H. Smith, Properties of dust in the Martian atmosphere from the imager on Mars Pathfinder, *J. Geophys. Res., 104*, 8987-9008, 1999.

Toon, O. B., J. B. Pollack, and C. Sagan, Physical properties of the particles composing the Martian dust storm of 1971-1972, *Icarus, 30*, 663-696, 1977.

Wilson, R. J., and K. P. Hamilton, Comprehensive model simulation of thermal tides in the Martian atmosphere, *J. Atmos. Sci., 53*, 1290-1326, 1996.

Wilson, R. J., and M. I. Richardson, The Martian atmosphere during the Viking mission, 1: Infrared measurements of atmospheric temperatures revisited, *Icarus*, in press, 2000.

Wolff, M. J., J. F. Bell III, P. B. James, R. T. Clancy, and S. W. Lee, Hubble Space Telescope observations of the Martian aphelion cloud belt prior to the Pathfinder mission: Seasonal and interannual variations, *J. Geophys. Res., 104*, 9027-9042, 1999.

Zurek, R. W., Solar heating of the Martian dusty atmosphere, *Icarus, 50*, 288-310, 1978.

Zurek, R. W., Martian great dust storms: An update, *Icarus, 50*, 288-310, 1982.

Zurek, R. W. and L. J. Martin, Interannual variability of planet-encircling dust storms on Mars, *J. Geophys. Res., 98*, 3247-3259, 1993.

P. R. Christensen, Geology Department, Arizona State University, Tempe, AZ 85287.

R. T. Clancy and M. J. Wolff, Space Science Institute, 3100 Marine Street, Suite A353, Boulder, CO 80303-1058. (clancyr@colorado.edu)

B. J. Conrath, Astronomy Department, Cornell University, Ithaca, NY 14853.

J. C. Pearl and M. D. Smith, Goddard Space Flight Center, Greenbelt, MD 20771.

B. J. Sandor, National Center for Atmospheric Research, Boulder, CO 80303.

R. J. Wilson, Geophysical Fluid Dynamics Laboratory (NOAA), Princeton, NJ 08542.

Received May 18, 1999; revised September 29, 1999; accepted October 5, 1999.

ORBITAL AND INTERANNUAL VARIABILITY OF THE GLOBAL MARS ATMOSPHERE. R.T. Clancy, Space Science Institute, P.O. Box 3075, Bald Head Island, NC 28461, clancyr@colorado.edu

Introduction: Studies of the Mars atmosphere over the past twenty years are largely based on a diverse set of Viking surface and atmospheric measurements collected between 1976-1981. The Viking-based view of the Mars atmosphere synthesized from these data is characterized by a constant background of vertically well mixed dust aerosol ($\tau \geq 0.5$), which increases by factors of ≥ 3 during the perihelion dust storm season [1]. Low-to-mid latitude atmospheric temperatures in all seasons are typically elevated by >15 K due to solar absorption by the suspended dust [2]. The global distribution of the atmospheric water column exhibits strong annual variation, which is primarily due to annual release of water from the exposed water ice residual cap and the receding CO_2 seasonal ice cap of the northern summer hemisphere. Polar sources of water vapor in the southern summer hemisphere are determined to be much smaller [3]. The warm atmospheric temperatures of the Viking model yield sub-saturation conditions for water vapor in the low-to-mid latitude atmosphere, to altitudes above 25 km in all seasons. As a result, Mars atmospheric photochemistry is characterized by high levels of catalytic radicals from water vapor photolysis (HO_x), and ice cloud formation is restricted to local phenomena (nighttime surface haze, topographic and wave driven discrete clouds) at low-to-mid latitudes. In the context of the Viking model, water ice clouds are not considered to influence the dynamical/radiative balance of the global Mars atmosphere [3].

A revision of this Viking-based climatology is merited on several accounts. The accumulation of ground-based and spacecraft observations over the past decade may be compared to the Viking and Mariner 9 observations to characterize the interannual variation of the Mars atmosphere in unprecedented detail. In addition, there are indications that the annual behavior of the global Mars atmosphere may not be well represented by the Viking model. Since 1988, ground-based millimeter observations (temperature and water profiling- [4,5]) and HST ultraviolet-visible imaging and spectroscopy [6-10] have determined colder (15-20K), cloudy, and less dusty conditions for the global Mars atmosphere relative to the Viking climatology, particularly for the minimum solar heating conditions around aphelion. Clancy et al. [5] identified a distinctive equatorial cloud belt in HST imaging during Mars aphelions in 1991, 1993, and 1995 (figure 1), and associated this phenomenon with the low altitudes (<10 km) of global water saturation and the latitudinal dependence of Hadley vertical advection during the northern summer season of aphelion (solar longitudes, L_s, of 40-140°). They further proposed that ice growth on dust aerosols leads to nonlinear feedback among atmospheric water vapor, temperature, cloud and dust distributions within the Mars atmosphere [11], and results in a much stronger orbital variation of the global Mars atmosphere than is reflected in the existing Viking climatology.

In the past two years, atmospheric measurements from Pathfinder [12,13] and Mars Global Surveyor [14-18], and reanalyses of Viking IRTM observations [18-20] have provided critical cross comparisons to contemporaneous ground-based observations and a reappraisal of atmospheric conditions that existed during the Viking period. These results are integrated with prior spacecraft and ground-based measurements to construct a revised description of the average annual variation of the Mars atmosphere, and a preliminary description of its interannual variability. Ultimately, MGS and the Mars Climate Observer (MCO) will define the spatial and seasonal variation of the global Mars atmosphere in detail that only dedicated atmospheric sounding from orbit can provide. A revision to the Viking model serves to consolidate the significant observational and data analysis developments over the past decade, and provide an interannual context of comparison for the flood of MGS and MCO atmospheric observations that has just begun.

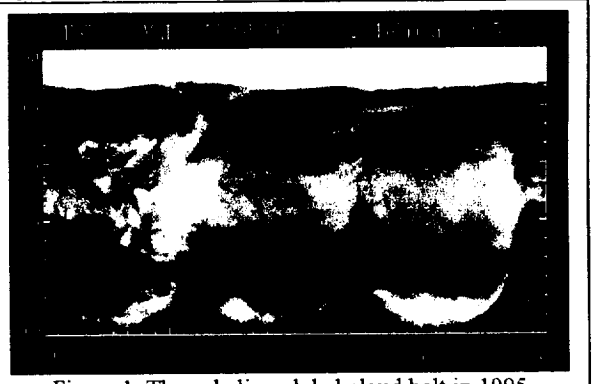

Figure 1: The aphelion global cloud belt in 1995

Atmospheric Temperatures: Figure 2 (from [18]) presents a broad comparison of observed low-to-mid latitude average temperatures at the 0.3 mbar pressure level (~30 km) versus Mars season. Temperature variations at this level are fairly representative of observed behavior over the extended Mars atmosphere (5-50 km), and can be compared among many data sets. For the purpose of these compari-

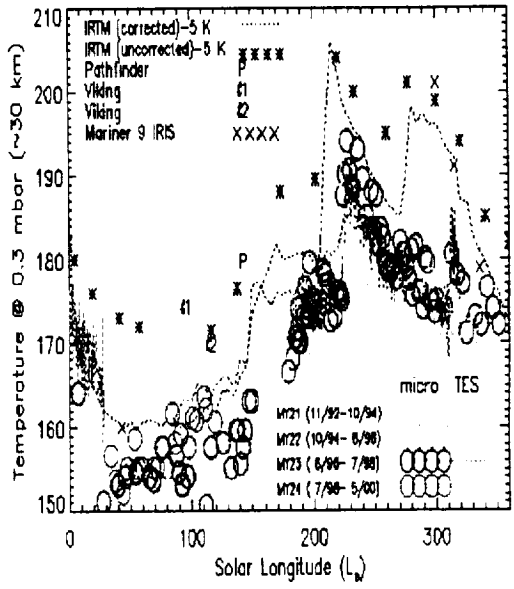

Figure 2: Orbital and interannual variations of low-to-mid latitude Mars atmospheric temperatures

sons, a solar longitude range 0-360° defines a Mars year, and April 11, 1955 (L_s=0°) is adopted as the beginning of year 1. In this arbitrary convention, the Mariner 9, Viking, Phobos, and Pathfinder missions occurred in years 9-10, 12-15, 19-20, and 23 respectively. By comparison, the 1992-1999 millimeter observations (circles, [5,18]) extend over years 21-24, and the 1997-1999 TES observations (dotted lines, [16]) over portions of years 23 and 24. The millimeter and TES measurements show excellent agreement over the 1997-1998 (L_s=190-30°) period of contemporaneous observations. The "uncorrected" IRTM temperatures (asterisks, [21]), which characterize the Viking model of Mars atmospheric behavior, fall 15 K above the temperatures retrieved by the millimeter measurements in all seasons. The "corrected" IRTM temperatures (dotted lines), resulting from the Wilson and Richardson [19] reanalysis of IRTM 15 μm radiances, are reasonably consistent with the seasonal and interannual dependence of atmospheric temperatures displayed by the millimeter measurements. It is also notable that the corrected 15 μm IRTM measurements of 20-30 km atmospheric temperatures are now 10-15K colder than the two Viking descent temperature profiles at L_s=96° and 116°. A similar conflict exists between the cold millimeter profiles and the warm Pathfinder descent temperature profile at L_s=140° in 1997 [18,22]. Within the millimeter data set, interannual variations in global-average atmospheric temperatures (by 5-20 K) are most prominent during the perihelion dust storm season (L_s=200-340°) and during the northern summer/fall period (L_s=100-200°). These are the same seasons for which millimeter and corrected IRTM temperatures exhibit their largest differences (10-20 K).

Global temperature increases associated with the onset of perihelion dust storms have been observed in the millimeter record in four consecutive Mars perihelions (years 20-23). Temperature increases of 15 K retrieved from millimeter and TES observations during the L_s=225° Noachis Terra regional dust storm in 1997 (year 23) are remarkably similar to the L_s=220° temperature increase in 1995 (year 22). However, the 25-30 K elevation of global temperatures determined from the L_s=254° millimeter measurement in 1995 (year 21) is more comparable to temperature increases which accompanied the Mariner 9 (year 9, [23]) and Viking (year 12) global dust storms. The detection of 4-5 small (5-10 K), yet distinct global temperature increases during the 1997 perihelion period suggests a fairly continuous spectrum of dust storm size and atmospheric forcing.

The early aphelion period (L_s=10-90°) presents the greatest degree of repeatability in Mars atmospheric temperatures, in terms of variability within the long-term millimeter data set and in comparison between the corrected IRTM and millimeter observations. Millimeter observations of aphelion atmospheric temperatures exist for years 14, 15, and 19-24. With the Wilson and Richardson correction for the Viking IRTM 15 μm radiances, all eleven observed Mars aphelions over the period year 9 to year 24, including the Mariner 9 period, have exhibited comparably cold atmospheric temperatures (to within 5 K) at this altitude level.

Dust and Ice Opacities: Figure 3 presents a comparison of visible dust column opacities at 0-30 N latitudes as derived from Mariner 9 IRIS (filled triangles-[24]) 9 μm dust opacities (1972, scaled by a factor-of-two); Viking lander 1 (+'s in year 12, X's in year 13-[1]) solar extinction measurements (1976-78); Viking IRTM (filled squares in year 12, filled diamonds in year 13-[25]) 9 μm dust opacities (1976-78, scaled by a factor-of-two); 1989 Phobos (asterisk) solar occultation [26]; 1995-97 Hubble Space Telescope imaging (HST-open triangles in years 20-22, open squares in year 23-[8]) imaging; and Pathfinder solar extinction imaging (solid line-[13]). Included in this figure are the average TES 9 μm dust opacities for the 0-30N latitude range in 1997-98 (filled circles-[15]), which have been scaled by a factor-of-two to present comparable visible dust opacities. Afternoon dust opacities from the Viking 1 lander

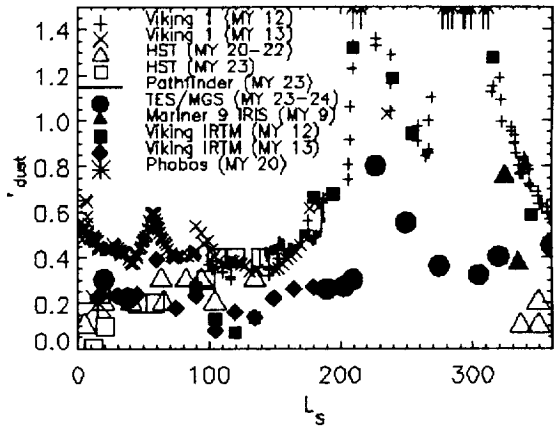

Figure 3: Orbital and interannual variations of low latitude dust opacity in the Mars atmosphere

record (smoothed with a running five point average) are presented, and the Viking and Pathfinder opacities are scaled to a surface pressure of 6.1 mbar (as are the TES opacities).

To first order, the Mars atmosphere in 1996-1998 (years 22-23) shows significantly lower dust loading relative to the 1976-77 Viking period (year 12). At L_s of 190-320° the 1997-98 TES measurements imply visible dust opacities at northern low latitudes which are 2-8 times lower than during the Viking period. TES dust measurements prior to the Noachis Terra storm show a factor of 2-3 less dust loading, compared to Viking 1 lander and IRTM measurements prior to the 1977a storm (0.3 versus 0.6-0.8 at L_s=180-205°. Notice, however, IRTM opacities at L_s=180-185° are significantly lower in year 13 than in year 12). Perihelion dust storm loading was particularly lower in 1997-98 relative to the 1977 period. The Noachis Terra dust storm of 1997 led to relatively modest dust loading in the northern hemisphere [13,14], as compared to the large dust opacities observed by both Viking landers and IRTM during the 1977a and 1977b dust storms (visible dust opacities of 0.6-0.8 versus 2-4). Although there are 30-50% increases in TES dust opacities between L_s=300° and 360° (which correspond to distinct L_s=310° and 340° atmospheric heating events, see figure 2), there was no second dust storm in 1997-98 comparable to the 1977b storm. Consequently, the L_s=280-320° seasonal range was much less dusty (3-8 times) in year 23 than during the equivalent season in year 12. Similarly, this season was less dusty than after the 1971 great dust storm (year 9-c.f., TES and IRIS), although by L_s=330-340° the 1972 dust loading had decayed to comparable levels observed in 1998.

The L_s=350-180° period of northern spring/summer exhibits a more complex variation among the TES, Viking

lander and IRTM, HST, and Phobos dust opacity measurements. At L_s=360° TES measurements are 2-3 times larger than the HST opacities, but are in reasonable agreement with the dust columns measured by Viking 1 and IRTM in 1977. However, the L_s=300-360° period in 1998 presents an increasing dust column due to the late season dust storm events at L_s=310° and 340° (figure 5). By comparison, the Viking 1977 and Mariner 9 1972 dust opacities over this L_s range decreased by a factor of 2-4, associated with the decay of the 1977b and 1971 storms. The TES opacities at L_s=20-40° are comparable to the Phobos (year 20), HST (years 20-23), and Viking IRTM (years 12-13) measurements for this season (τ_{vis}~0.1-0.3), and roughly a factor of 2 less than the Viking lander 1 opacities. The northern summer season at L_s=140-180° shows good agreement among the Viking lander and Pathfinder observations, whereas the Viking IRTM and MGS TES measurements in 1976-78 and 1997 are typically lower by a factor-of-two.

The differences between the 1978 Viking lander and IRTM opacities over L_s=10-180° (year 13) and the 1997 TES and Pathfinder measurements at L_s=190° (year 23) are particularly surprising as these are contemporaneous data sets. The unrecognized contribution of large aphelion cloud opacities in the lander aerosol measurements may account for much of this disagreement. The lander analyses effectively assume negligible cloud opacities during the daytime, consistent with the Viking-based model of a warm, dusty atmosphere, whereas the IR measurements spectroscopically discriminate cloud and dust opacities. HST imaging during the past 5 aphelions (years 20-24) clearly identifies the presence of daytime cloud opacities of 0.1-0.4 (figure 1). The Wilson and Richardson [19] reanalysis of Viking IRTM 15 μm measurements (figure 2) now implies comparable aphelion saturation conditions for the Viking period, and recent analysis of IRTM 11 μm radiances identifies the presence of a global aphelion cloud belt during the Viking period (Tampari et al., 1997). Finally, TES mapping of dust and ice opacities during the 1999 aphelion (L_s=110°) provides a striking display of the aphelion cloud belt in the 11-12 μm water ice band [17]. These TES measurements imply that visible cloud opacities can exceed visible dust opacities (τ_{dust}~0.1) within the aphelion cloud belt.

It is also worth noting the possibility that fine CO_2 ice clouds may be a relatively common low latitude phenomenon within the mesosphere (60-100 km altitudes) of Mars. Submillimeter measurements of temperatures at the 70-80 km altitude region indicate dayside average temperatures only 10 K above CO_2 saturation conditions during the equinoctal seasons [22]. The presence of CO_2 ice clouds in the mesosphere was proposed as an explanation of the 4.3 μm CO_2 ice spectral line scattering identified by Mariner 6 and 7 IRS limb observations at L_s=200° in 1969 [32]. In addition, very cold regions over the 60-90 altitude range were observed to fall below CO_2 saturation conditions during the Pathfinder descent [12].

Water Vapor and Photochemistry: Figures 4 and 5 present two aspects of Mars atmospheric water behavior which may be considered as significant modifications to the Viking model. In figure 4, the latitudinal dependence of Mars atmospheric water column during the northern vernal equinox is presented for four separate Mars years. This comparison of Viking MAWD observations [27] to recent ground-based visible [28,29] and centimeter [30] measurements provides one of the more compelling cases for strong interannual variability of Mars atmospheric water. A factor of >4 interannual variation is implied over the 1988-1994 period for this season of minimum atmospheric water abundance [29,30]. By comparison, ground-based and Viking observations during the northern spring/summer season of maximum atmospheric water abundance (L_s=20-120°) show relatively modest interannual variability [29,31].

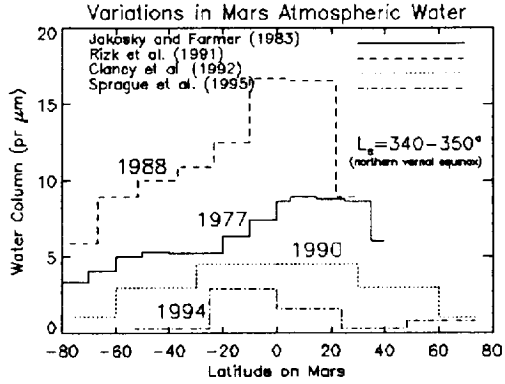

Figure 4: The interannual variation of Mars atmospheric water in late northern winter

Figure 5 presents the behavior of water vapor saturation conditions in the low-to-mid latitude Mars atmosphere as a function of season [5]. The colder atmospheric conditions returned by the millimeter observations (dashed lines, computed for 3 levels of atmospheric water abundance) lead to much lower altitudes of water saturation relative to the Viking climatology (solid lines). Differences between these models in the perihelion season reflect interannual variability of dust storm activity in this season. TES observations show correlations in 30-50 km water clouds with dust storm activity in this season in 1997 [17]. Differences between the Viking and microwave (millimeter) based models during the aphelion period are a consequence of the warm bias in the Viking model (figure 2). Millimeter HDO and centimeter H_2O spectral line observations confirm the presence of very low saturation altitudes around 1993 and 1995 Mars aphelions [5]. The resulting orbital variation in water vapor densities at altitudes above 10 km forces large orbital variations in atmospheric photochemistry [33], as water photolysis products (OH, HO_2, H_2O_2) are the primary catalytic reagents for ozone destruction in the Mars atmosphere [32]. HST

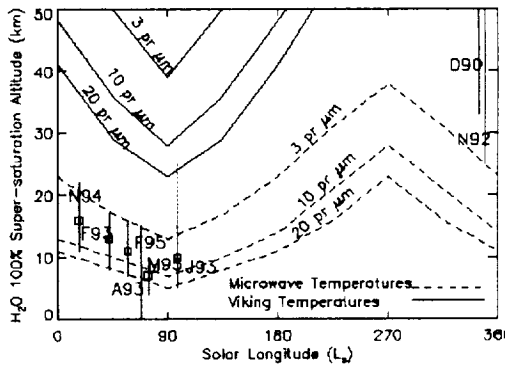

Figure 5: Orbital variation of low-to-mid latitude water vapor saturation conditions in the Mars atmosphere

ultraviolet spectroscopic determinations of Mars ozone column distributions show that low-to-mid latitude ozone column increases by a factor-of-two during the aphelion period [9,10]. This increase in the ozone column corresponds to factors of 3-10 in ozone density increases above 10 km altitudes, which result from the removal of vapor vapor by saturation and cloud formation around the aphelion season [33].

Revised Atmospheric Climatology: The strong (40%) orbital variation in solar flux incident on Mars leads to distinct aphelion and perihelion climates, which occur (in the current epoch) around the northern and southern summer solstices, respectively. Annual variations in the general circulation of the atmosphere and the growth/recession of the polar caps are more closely tied to the obliquity of Mars. In contrast, annual and interannual variations of low-to-mid latitude temperatures, dust and ice aerosol loading, and composition (water, ozone) are more closely tied to aphelion-perihelion orbital variations. The following summary of annual and interannual variations in the global Mars atmosphere employs this orbital methodology.

1) The perihelion season (L_s=200-340°) experiences regional-to-global dust storms every Mars year. Average global dust opacities are significantly reduced during years of regional (τ_{vis}=0.5-1.0) versus global (τ_{vis}=2-4) dust storms. Global dust storms (as in 1971 and 1977) may occur in roughly one-half to one-third of Mars years. Multiple dust storms of smaller extent also occur throughout the L_s=200-340° period. In all cases, from global to sub-regional scale, these dust storms onset as discrete events, leading to 5-30 K global increases in atmospheric temperatures over extended altitudes (0-50 km) and with remarkably abrupt timescales (1-2 days). Atmospheric water abundances in this southern solstice season are several times less than observed during the northern summer solstice. However, they are also poorly determined from existing observations, and may or may not show influences from south polar reservoirs and significant interannual variability. Large (200%) enhancements in water columns appear within the Hellas and Argyre basins over L_s=245-275°, and may strongly influence the latitudinal distribution of atmospheric water in this season. The warm atmospheric conditions of the perihelion period present subsaturation conditions for atmospheric water to high altitudes (35-60 km, where variable, optically thin water ice clouds are present), high levels of photochemical radicals (such as NO_x and HO_x), and minimum levels of atmospheric ozone.

2) The aphelion atmosphere (L_s=20-140°) is most repeatable in temperature, water column, and aerosol conditions from year-to-year. The long-standing Viking model of atmospheric temperature, cloud, and dust behavior is an inaccurate description of this season in particular, even for the Viking period of observation. The aphelion period is characterized global conditions of cold atmospheric temperatures (20-30 K cooler than during perihelion), low altitudes of water vapor saturation (<10 km), enhanced cloud opacities (τ_{vis} = 0.1-0.5, including a distinctive low latitude cloud belt), and low dust opacities (τ_{vis} = 0.1-0.3). As the northern summer season progresses beyond L_s=100°, dust and cloud opacities remain similar to aphelion conditions but atmospheric temperatures exhibit increased temporal (and possibly spatial) variability relative to the L_s=20-100° period. The global distribution of atmospheric water vapor in this season is dominated by northern residual and seasonal cap sources, and does not appear to exhibit strong interannual variability. The low altitudes of global water saturation in this season lead to minimum levels of photochemical radicals and maximum columns of atmospheric ozone (apart from the polar regions).

3) The transitional seasons of L_s=340-20° (northern vernal equinox) and L_s=140-200° (southern vernal equinox) are characterized by intermediate interannual variability in global atmospheric temperatures (5-15 K), relative to the constant aphelion and highly variable perihelion periods. Year-to-year variations of temperature (5-10 K) and dust conditions (τ_{vis}=0.1-0.6) within the L_s=340-20° period reflect year-to-year variations in late perihelion season dust storm activity. Atmospheric water vapor exhibits very large interannual variations during this period (average water columns of ~1 to >10 pr μm), and may indicate comparable interannual variability in southern hemispheric water during the perihelion season when the behavior of atmospheric water is not well observed. Cloud opacities begin to increase and descend to lower altitudes.

Year-to-year variations in global atmospheric temperatures over the L_s=140-200° period are characterized by a distinctive 10-15 K increase in 20-30 km atmospheric temperatures at L_s=140-150° in 1976 and 1978. This behavior is not evident in the 1992-1998 millimeter observations, but current millimeter observations show a trend towards such warmer conditions by L_s=120° in 1999. No obvious increase in dust column opacity accompanies this late northern summer rise in global atmospheric temperatures, suggesting that an increasing vertical extent of the dust heating may contribute to this behavior. This behavior may also reflect an increasing altitude for the formation of water ice clouds, which may still present signifcant opacities. Very cold atmospheric temperatures at 60-100 km altitudes may also lead to local formation of CO_2 ice clouds during the equinoxes.

References: **[1]** Colburn et al. (1989) *Icarus*, 79, 159-189. **[2]** Pollack et al. (1979) *JGR*, 84, 2929-2945. **[3]** Jakosky and Haberle (1992) *MARS*, ed. Kieffer et al, 1151–1154969-1016. **[4]** Clancy et al. (1990) *JGR*, 95, 14543-14554. **[5]** Clancy et al. (1996) *Icarus*, 122, 36-62. **[6]** James et al. (1994) *Icarus*, 109, 79-101. **[7]** James et al. (1996) *JGR*, 101, 18883-18890. **[8]** Wolff et al. (1999) *JGR*, in press. **[9]** Clancy et al. (1996) *JGR*, 101, 12777-12783. **[10]** Clancy et al. (1999) *Icarus*, 138, 49-63. **[11]** Rodin et al. (1999) *Icarus*, in review. **[12]** Schofield et al. (1998) *Science*, 278, 1752-1758. **[13]** Smith et al. (1998) *Science*, 278, 1758-1768. **[14]** Christensen et al. (1998) *Science*, 279, 1692-1698. **[15]** Smith et al. (1999) submitted to *JGR*. **[16]** Conrath et al. (1999) submitted to JGR. **[17]** Pearl et al. (1999) submitted to *JGR*. **[18]** Clancy et al. (1999) submitted to *JGR*. **[19]** Wilson and Richardson (1999) *JGR*, in review. **[20]** Tamppari et al. (1996) *Bull. Amer. Astron Soc.* 29, 961. **[21]** Kieffer et al. (1977) *JGR*, 82, 4249-4292. **[22]** Clancy and Sandor (1998) *GRL*, 25, 489-492. **[23]** Conrath (1975) *Icarus*, 24, 36-46. **[24]** Fenton et al. (1997) *Icarus*, 130, 115-124. **[25]** Martin (1986) *Icarus*, 66, 2-21. **[26]** Chassefiere et al. (1992) *JGR*, 100, 5525-5540. **[27]** Jakosky and Farmer (1982) *JGR*, 87, 2999-3019. **[28]** Rizk et al. (1991) *Icarus*, 90, 205-213. **[29]** Sprague et al. (1995) *JGR*, 101, 23229-23241. **[30]** Clancy et al. (1992) *Icarus*, 100, 48-59. **[31]** Jakosky and Barker (1984) *Icarus*, 57, 322-334. **[32]** Herr and Pimental (1970) *Science*, 167, 47-49. **[33]** Clancy and Nair (1996) *JGR*, 101, 12785-12790. **[34]** Parkinson and Hunten, (1972), *J. Atmos. Sci.*, 29, 1380-1390.